

# Adult interfollicular tumour-initiating cells are reprogrammed into an embryonic hair follicle progenitor-like fate during basal cell carcinoma initiation

Khalil Kass Youssef<sup>1</sup>, Gaëlle Lapouge<sup>1</sup>, Karine Bouvrée<sup>1</sup>, Sandrine Rorive<sup>2,3</sup>, Sylvain Brohée<sup>1,4</sup>, Ornella Appelstein<sup>1,4</sup>, Jean-Christophe Larsimont<sup>1</sup>, Vijayakumar Sukumaran<sup>1</sup>, Bram Van de Sande<sup>5</sup>, Doriana Pucci<sup>1</sup>, Sophie Dekoninck<sup>1</sup>, Jean-Valery Berthe<sup>6</sup>, Stein Aerts<sup>5</sup>, Isabelle Salmon<sup>2,3</sup>, Véronique del Marmol<sup>7</sup> and Cédric Blanpain<sup>1,8,9</sup>

**Basal cell carcinoma, the most frequent human skin cancer, arises from activating hedgehog (HH) pathway mutations; however, little is known about the temporal changes that occur in tumour-initiating cells from the first oncogenic hit to the development of invasive cancer. Using an inducible mouse model enabling the expression of a constitutively active Smoothed mutant (SmoM2) in the adult epidermis, we carried out transcriptional profiling of SmoM2-expressing cells at different times during cancer initiation. We found that tumour-initiating cells are massively reprogrammed into a fate resembling that of embryonic hair follicle progenitors (EHFPs). Wnt/ $\beta$ -catenin signalling was very rapidly activated following SmoM2 expression in adult epidermis and coincided with the expression of EHFP markers. Deletion of  $\beta$ -catenin in adult SmoM2-expressing cells prevents EHFP reprogramming and tumour initiation. Finally, human basal cell carcinomas also express genes of the Wnt signalling and EHFP signatures.**

Cancer is thought to result from the accumulation of mutations in the progeny of a single cell. However, as tumours or their precursor lesions are usually analysed when the tissues already show pathological features, little is known about tumour initiation. The cell lineages at the origin of most cancers are still unknown, and the molecular changes occurring in tumour-initiating cells remain poorly characterized. A detailed temporal and molecular analysis of tumour-initiating cells from the first oncogenic mutation to the formation of invasive tumours is required to understand the mechanisms controlling the early steps of cancer development.

Basal cell carcinoma (BCC) results from mutations leading to constitutive activation of the HH pathway, either through Patched loss of function or by activating mutations in the Smoothed (*Smo*) gene<sup>1</sup>. Different mouse models of BCC recapitulate well the main features of human BCC (ref. 2). Using mice conditionally expressing a constitutively active mutant of *Smo* (SmoM2), which

induces BCC-like lesions in human and mouse<sup>3,4</sup>, we and others have demonstrated that, during homeostasis, SmoM2-induced BCC-like tumours arise most frequently from adult progenitor cells residing in the adult interfollicular epidermis<sup>5,6</sup> (IFE). The BCC-initiating cells start expressing hair follicle markers before progressing into BCC, demonstrating that the expression of differentiation markers by tumour cells can be misleading in extrapolating their cellular origin<sup>5</sup>.

BCCs express hair follicle markers such as P-cadherin, Krt17, CDP, Lgr5 or Sox9 (refs 7–13); however, the extent of their resemblance to hair follicles and the temporal appearance and mechanisms regulating hair follicle marker expression during BCC initiation are unclear. It is also unknown whether the hair follicle markers expressed in BCCs are more representative of an embryonic rather than an adult stage. The temporally regulated expression of SmoM2 in adult epidermis and the ability to track and isolate the cell at the origin of SmoM2-induced BCC offer a unique opportunity to dissect the

<sup>1</sup>IRIBHM, Université Libre de Bruxelles (ULB), 808 route de Lennik, 1070 Brussels, Belgium. <sup>2</sup>Department of Pathology, Erasme Hospital, Université Libre de Bruxelles, Brussels 1070, Belgium. <sup>3</sup>DIAPATH — Center for Microscopy and Molecular Imaging (CMMI), Gosselies 6041, Belgium. <sup>4</sup>Computer Science Department, Université Libre de Bruxelles, Boulevard du Triomphe, CP 212, 1050 Brussels, Belgium. <sup>5</sup>Laboratory of Computational Biology, Center for Human Genetics, K.U. Leuven, Leuven 3000, Belgium. <sup>6</sup>Department of Plastic Surgery, Erasme Hospital, Université Libre de Bruxelles, Brussels 1070, Belgium. <sup>7</sup>Department of Dermatology, Erasme Hospital, 1070 Brussels, Belgium. <sup>8</sup>WELBIO, Université Libre de Bruxelles (ULB), 808 route de Lennik, 1070 Brussels, Belgium. <sup>9</sup>Correspondence should be addressed to C.B. (e-mail: cedric.blanpain@ulb.ac.be)

temporal and molecular changes associated with cancer initiation and progression in this mouse model.

Here, we carried out transcriptional profiling of SmoM2-expressing IFE cells at different stages of tumour initiation and found that adult tumour-initiating cells undergo profound and rapid reprogramming into an EHFP-like fate. One of the earliest events following SmoM2 expression is the cell-autonomous activation of the Wnt/ $\beta$ -catenin pathway through the upregulation of a set of Wnt ligands, receptors and downstream transcription factors. Deletion of  $\beta$ -catenin from adult SmoM2-expressing cells blocks adult IFE cell reprogramming into EHFP-like cells and tumour initiation. Similar EHFP and Wnt signatures are found in a prospective cohort of human BCCs, suggesting that the process underlying tumour initiation may operate in human invasive BCCs irrespective of the mutated oncogene or histological subtypes.

## RESULTS

### Reprogramming of adult interfollicular cells into an EHFP fate following oncogenic hedgehog signalling

We induced the expression of SmoM2 in the basal cells of the epidermis by administering tamoxifen (TAM) to four-week-old K14CREER/Rosa-SmoM2 mice and carried out gene expression profiling of fluorescence-activated cell sorting (FACS)-isolated SmoM2-expressing basal interfollicular cells (YFP+/ $\alpha$ 6HCD34-: YFP, yellow fluorescent protein), at three days and one (normal histology), four (dysplastic lesion) and ten (invasive BCC) weeks after TAM administration (Fig. 1a–c). Comparison of the transcriptional profiles of SmoM2-expressing cells with FACS-isolated cells ( $\alpha$ 6HCD34-) from littermate control mice determined the ‘SmoM2 signature’, a list of genes differentially regulated by SmoM2 expression in IFE cells more than twofold in at least two independent biological replicates (Methods).

To determine the transcriptional changes in oncogene-expressing cells that led to hair follicle marker expression, we compared the genes differentially regulated by SmoM2 in adult IFE cells with genes known to be preferentially expressed by adult CD34+ hair follicle bulge stem cells when compared with IFE cells (‘bulge stem cell signature’)<sup>14</sup> and EHFPs when compared with IFE cells (‘EHFP signature’)<sup>15</sup>. Three days after TAM administration, when the first SmoM2–YFP cells can be detected and isolated by FACS, only 4% of the SmoM2-upregulated genes overlap with the EHFP or bulge stem cell signatures ( $P$ -values 0.07 and 0.06 respectively; Supplementary Fig. S1b). As early as one week after TAM administration, 24.7% of the EHFP signature genes were upregulated by SmoM2 expression ( $P = 1.6 \times 10^{-84}$ ), in contrast to only 11.6% of the bulge stem cell signature genes ( $P = 6.7 \times 10^{-23}$ ; Fig. 1d). This overlap increased with time, and four weeks after SmoM2 expression 45.2% of the EHFP signature genes were upregulated in adult IFE cells ( $p = 5.2 \times 10^{-141}$ ) whereas the overlap with the bulge stem cell signature was only 30.7% at this time ( $p = 1.1 \times 10^{-67}$ ). Among these genes, 33.8% were commonly upregulated by both EHFPs and adult bulge stem cells (Fig. 1d). Similarly, 32% of the SmoM2-downregulated genes were also downregulated in the EHFP signature (Fig. 1e), suggesting that SmoM2 represses genes preferentially expressed by the basal IFE cells. Gene set enrichment analysis (GSEA) scores<sup>16</sup>, which take into account the fold change of the 46,000 probes investigated here, showed a

better enrichment and greater statistical significance between EHFP and SmoM2 signatures than between bulge stem cell and SmoM2 (Supplementary Fig. S2a,b).

These data show that SmoM2 expression in adult IFE cells promotes the expression of an important proportion of EHFP signature genes, indicating the rapid transcriptional reprogramming of SmoM2 tumour-initiating IFE cells into an EHFP-like fate as early as one week after oncogene expression, when the oncogene-expressing cells still seem histologically normal and have undergone few rounds of cell division.

Using quantitative polymerase chain reaction with reverse transcription (qRT–PCR) analysis of FACS-isolated IFE cells at different times after SmoM2 expression, we confirmed the rapid and sustained increased expression of genes downstream of HH signalling such as *Gli1/2*, *Ptch1/2* and *Hhip* and the progressive upregulation of hair follicle markers expressed in human BCC such as *Lgr5* (ref. 12) or *Sox9* (refs 10,11; Fig. 2a). Key transcriptional regulators of embryonic hair follicle development such as *Runx1* (refs 17,18) or *Lhx2* (ref. 15) and many genes preferentially induced in EHFPs (ref. 15) were also upregulated (Fig. 2a). Immunostaining analysis demonstrated that few of these markers were significantly expressed in IFE SmoM2-expressing cells one week after TAM administration (Fig. 2b–e). However, at four weeks, SmoM2-expressing IFE cells did not continue to differentiate into suprabasal K10-expressing cells, but instead accumulated into dysplastic lesions resembling embryonic hair follicles that grew downward and expressed EHFP markers including P-cadherin, and transcription factors regulating embryonic hair fate decision such as *Lhx2* and *Cux1* (refs 15,19). These markers continued to be expressed at the leading edge of invasive BCC (Fig. 2b–g).

Bulge stem cells have been shown to initiate BCC formation following *Ptch1* deletion<sup>20,21</sup>, in particular after wounding<sup>21</sup>. To assess the contribution of IFE cells in Patched-induced BCC, we administered 1 mg TAM to one-month-old K14CREER/*Ptch1* flox/flox (ref. 22) mice and analysed the paw epidermis, which is completely devoid of hair follicles. Four weeks following Patched deletion many early tumorigenic lesions were visible throughout the IFE, and expressed the same embryonic hair follicle markers including *Lhx2*, *Cux1*, P-cadherin and downregulated the expression of K1 (Fig. 3a–f). At nine weeks, many of these lesions progressed into more invasive BCC, with branching morphology similar to that of SmoM2-induced BCC (Fig. 3a–g). These data indicate that IFE progenitors are able to initiate BCC following Patched deletion and also undergo an EHFP-like reprogramming before progressing into invasive BCC.

### Rapid activation of Wnt/ $\beta$ -catenin signalling in adult interfollicular cells following oncogenic SmoM2 expression

Functional annotation clustering of the genes upregulated by SmoM2 expression one week after TAM administration using DAVID software (<http://david.abcc.ncifcrf.gov/>) revealed a strong enrichment of genes belonging to the Wnt/ $\beta$ -catenin pathway (4.01-fold,  $P = 3.74 \times 10^{-7}$  for canonical Wnt receptor signalling pathway GO:0060070; Supplementary Fig. S3a,b and Table S1). Transcriptional analysis of the SmoM2-expressing IFE cells using qRT–PCR confirmed the very rapid (*Wnt6*, *Wnt7b* and *Lef1* were upregulated three days after TAM) and sustained expression of specific Wnt/ $\beta$ -catenin pathway components, including Wnt ligands (for example *Wnt6*, *Wnt7a*, *Wnt7b*), receptors (for example *Fzd2*, *Fzd3*, *Fzd7*), downstream transcription factors (for

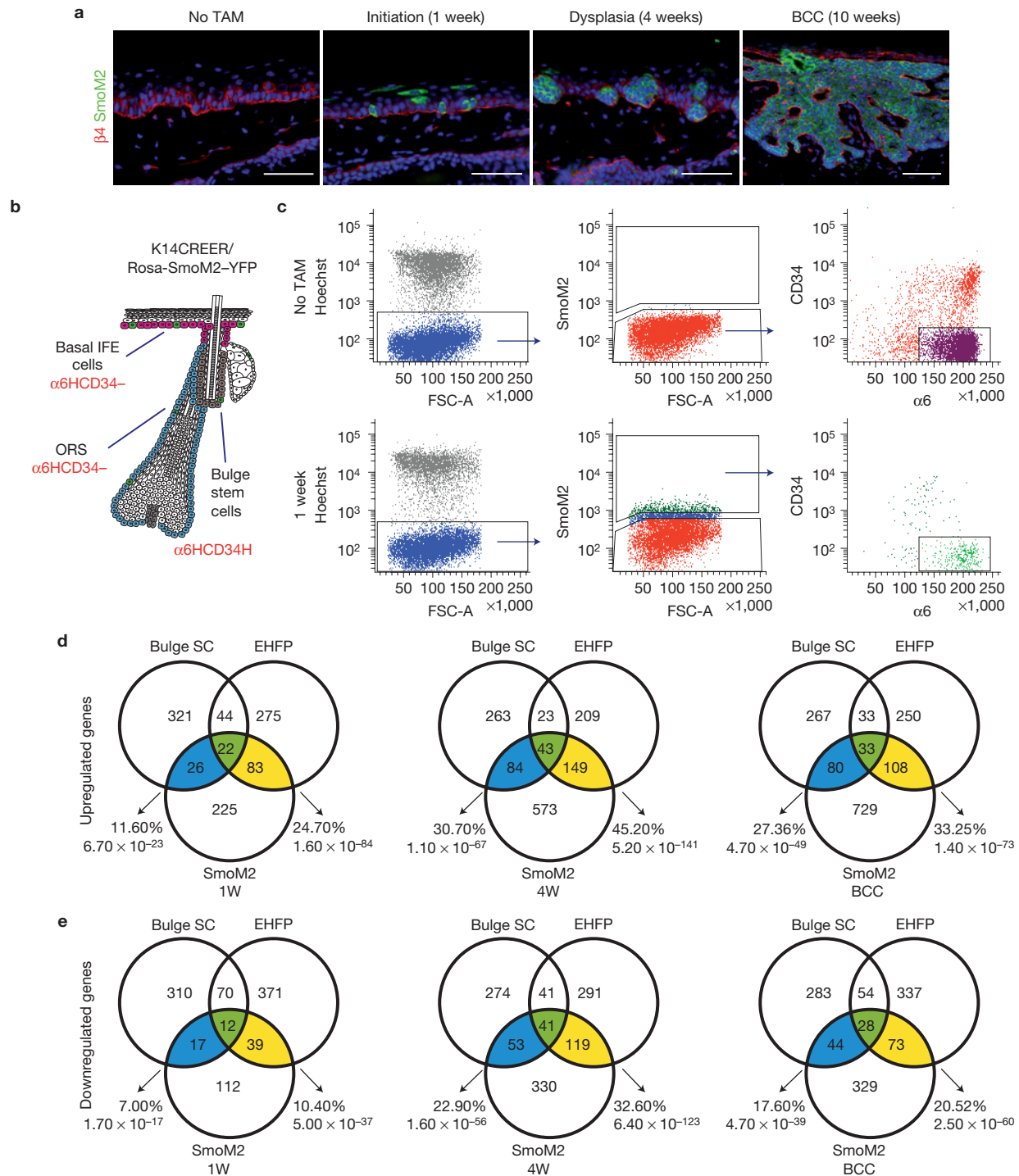


**Figure 1** Transcriptional analysis of FACS-isolated SmoM2-expressing cells at different times following oncogene expression. **(a)** Immunostaining of the tail epidermis before and one, four and ten weeks after 1 mg TAM administration to K14CREER/Rosa-SmoM2-YFP mice, showing the temporal histological changes occurring in basal IFE cells following SmoM2 expression. **(b)** Scheme representing the pattern of SmoM2 expression following TAM administration to K14CREER/Rosa-SmoM2-YFP mice and the markers ( $\alpha 6\text{HCD}34^-$ ) used to isolate SmoM2 tumour-initiating cells (basal IFE and infundibulum cells) by FACS. **(c)** Cell-sorting strategy to isolate tumour-initiating cells at different times following oncogene expression. After cell debris and doublet exclusion, living (DAPI $^-$ ), SmoM2+ (YFP $^+$ ),  $\alpha 6\text{HCD}34^-$  cells were isolated by FACS with high purity. The genes differentially regulated more than twofold in biological triplicates

on SmoM2 expression in  $\alpha 6\text{HCD}34^-$  cells were determined by microarray analysis ('SmoM2 signature'). **(d,e)** Venn diagrams showing the similarities and the differences between the genes differentially upregulated **(d)** and downregulated **(e)** by SmoM2 in adult IFE cells ( $\alpha 6\text{HCD}34^-$ ) and the genes belonging to the adult hair follicle bulge stem cell (SC) signature<sup>14</sup> or the EHFP signature<sup>15</sup> one, four and ten weeks after SmoM2 expression. The number of genes regulated by SmoM2 expression that overlapped with the EHFP signature (yellow) is more important than those that overlapped with the adult bulge stem cell signature (blue), or with the genes commonly regulated in both adult bulge stem cell and EHFP signatures (green). Arrows indicate the percentages and the hypergeometric *P*-values of the overlaps between SmoM2 signature and the adult bulge stem cell signature or the EHFP signature. Scale bars, 50  $\mu\text{m}$ . ORS, outer root sheath.

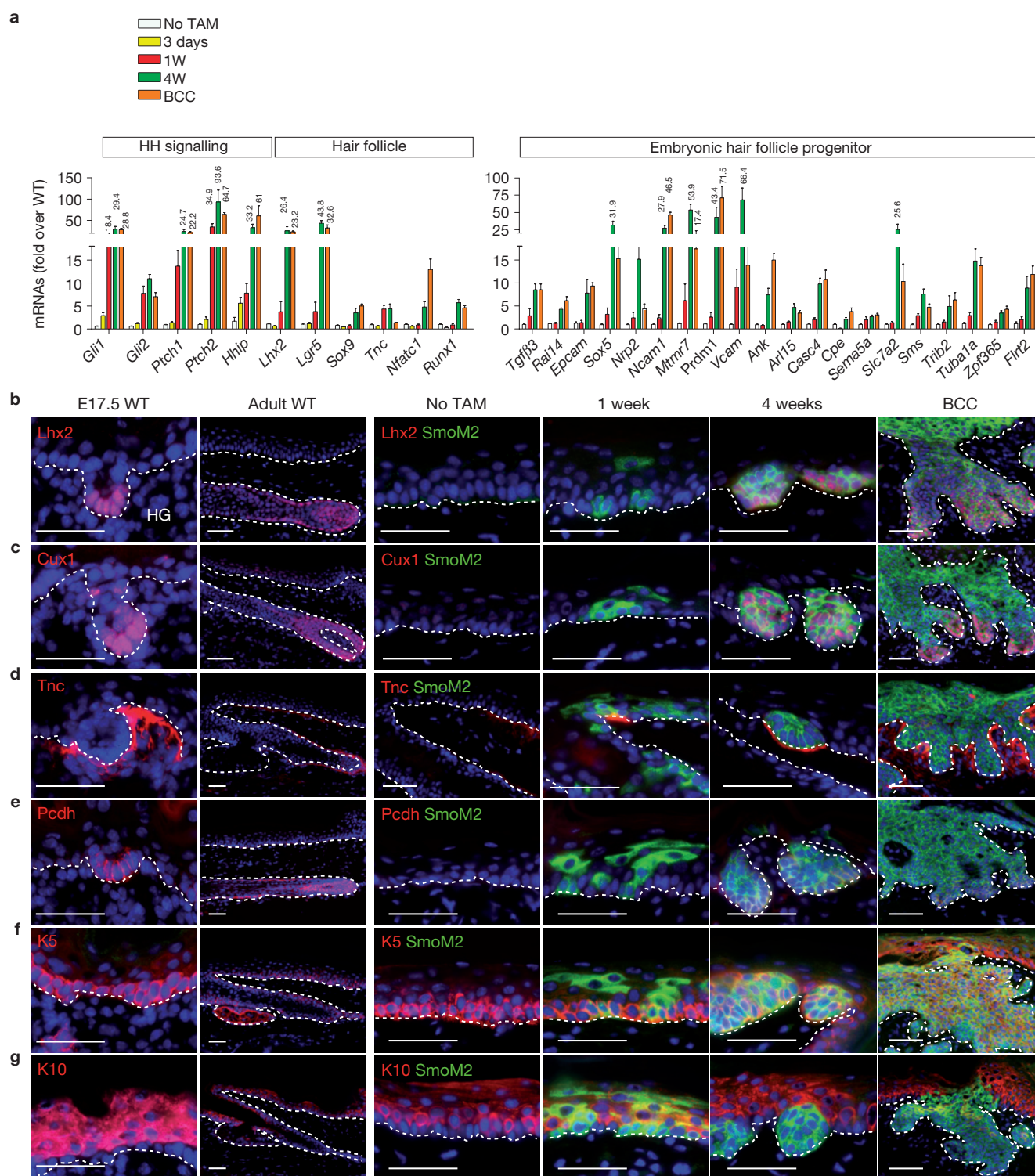


**Figure 2** Reprogramming of adult interfollicular cells into EHFPs following SmoM2 expression. **(a)** Relative mRNA expression of HH target genes, hair follicle markers and genes belonging to the EHFP signature genes in FACS-isolated  $\alpha 6HCD34^+$  cells from wild type control (no TAM,  $n=8$ ), and K14CREER/Rosa-SmoM2-YFP mice three days ( $n=6$ ) and one ( $n=6$ ), four (dysplasia,  $n=4$ ) and ten (BCC,  $n=6$ ) weeks after TAM administration. The bars represent the mean values of the relative mRNA expression of different biological replicates and the error bars represent s.e.m. WT, wild type. **(b-g)** Immunostaining of hair follicle

and epidermal markers in skin sections during embryonic development (E17.5), adult wild-type skin and one, four (dysplasia) and ten (BCC) weeks after SmoM2 expression in the adult epidermis. SmoM2-YFP expression is represented in green, whereas the EHFP and hair follicle markers Lhx2 **(b)**, Cux1 **(c)**, Tnc **(d)** and Pcdh **(e)**, the basal marker K5 **(f)** and the differentiated marker K10 **(g)** are represented in red. These data show that the early SmoM2-induced dysplastic lesions in the adult IFE resemble EHFPs morphologically and biochemically. Scale bars, 50  $\mu\text{m}$ . HG, hair germ.

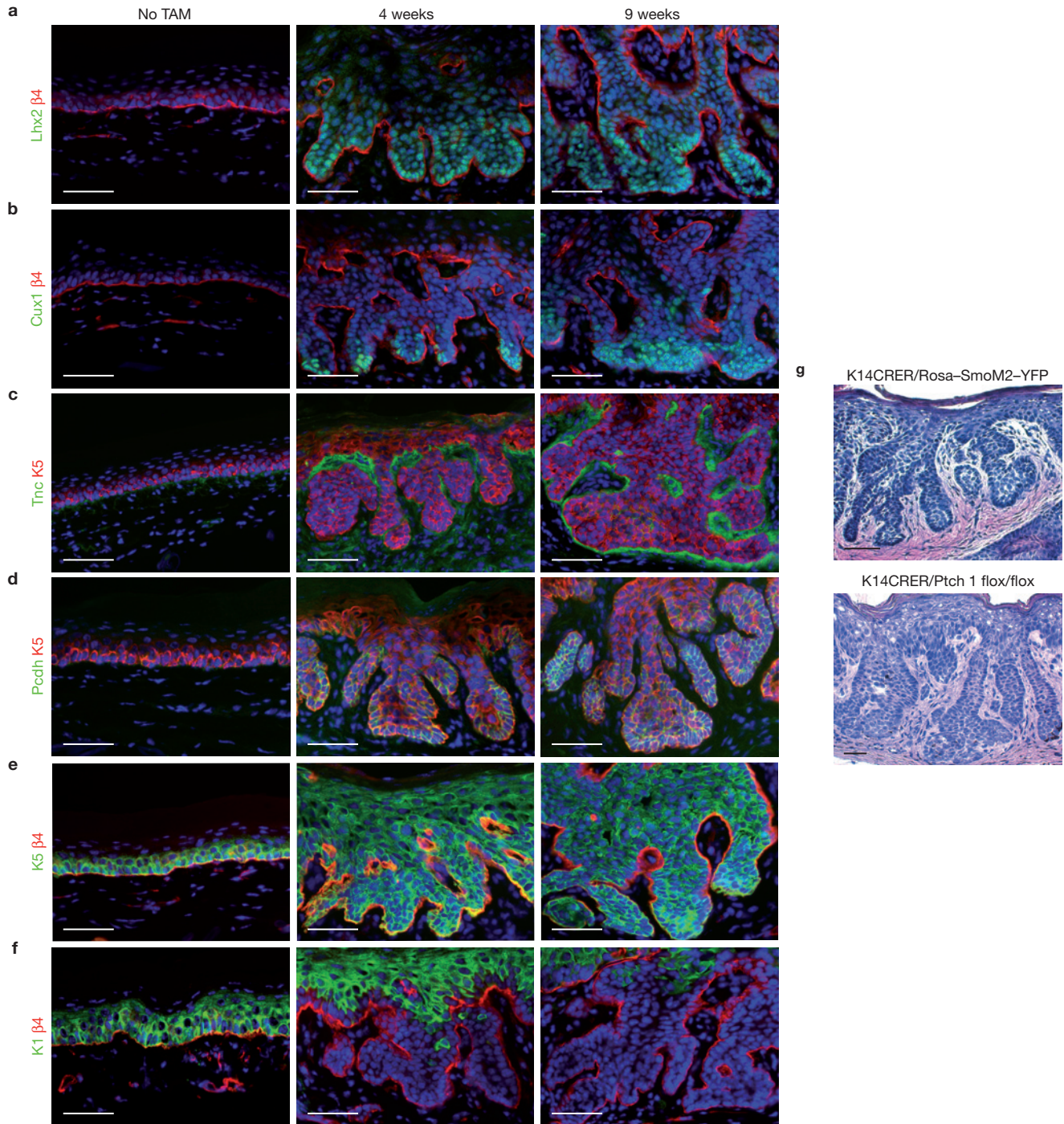


**Figure 3** Reprogramming of adult interfollicular cells into EHFPs following *Ptch1* deletion from the hairless paw epidermis. (a–f) Immunostaining of hair follicle and epidermal markers in adult paw epidermis of K14CREER/*Ptch1* flox/flox mice before and four and nine weeks after 1 mg TAM administration. EHFP and hair follicle markers Lhx2 (a), Cux1 (b), Tnc (c) and Pcdh (d), the basal marker K5 (e) and the differentiated marker K10 (f) are represented

in green. These data show that the early tumorigenic lesions occurring following *Ptch1* deletion from the adult IFE express EHFP marker before progressing into BCC. (g) Haematoxylin and eosin staining of BCCs in K14CREER/*Rosa-SmoM2-YFP* tail epidermis and K14CEER/*Ptch1* flox/flox paw epidermis nine weeks after TAM administration, showing their very similar histological appearances. Scale bars, 50  $\mu$ m.

example *Lef1*) and known target genes in the epidermis (for example *Biglycan*; ref. 23; Fig. 4a) and in other cell types (for example *Lgr5*, *Grem1*, *Tnfrsf11b*, *Nrcam* or *Vcan*).

During embryonic development Wnt/ $\beta$ -catenin signalling is active in EHFPs and the underlying mesenchyme<sup>24</sup>, as shown by the presence of nuclear  $\beta$ -catenin and *Lef1* (Fig. 4b,i), whereas in the adult epidermis

Wnt/ $\beta$ -catenin activity is restricted to hair follicle lineages<sup>24</sup> and mesenchymal dermal papillae<sup>25,26</sup> (Fig. 4c,j). Under physiological conditions no Wnt/ $\beta$ -catenin signalling activity is observed in adult IFE cells, as shown by the presence of membrane-associated, but not nuclear,  $\beta$ -catenin and by the absence of *Lef1* expression (Fig. 4d,k). In contrast, one week after *SmoM2* expression, nuclear  $\beta$ -catenin

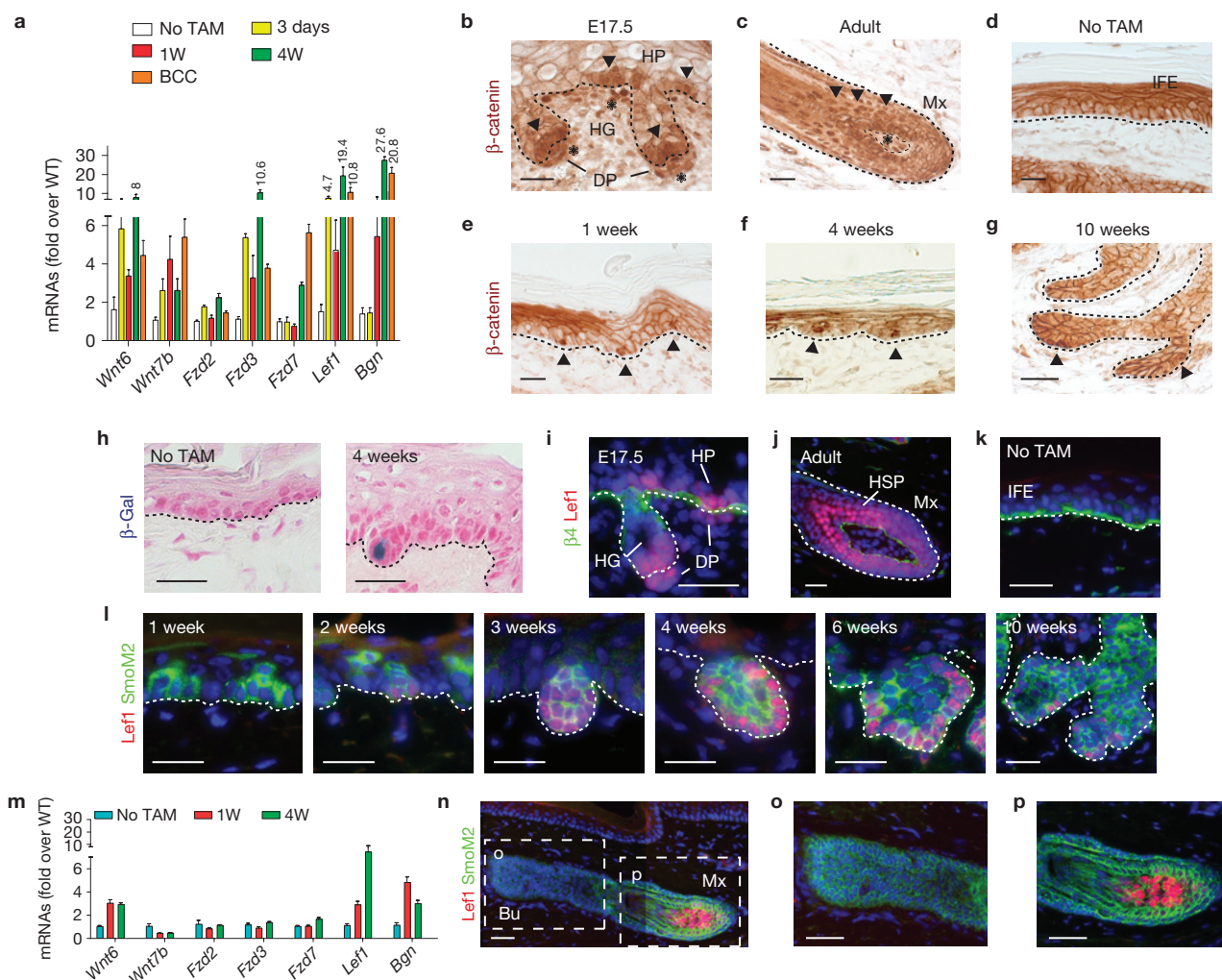


**Figure 4** Wnt/ $\beta$ -catenin signalling is rapidly activated in adult interfollicular cells following SmoM2 expression. **(a)** Relative mRNA expression of genes of Wnt/ $\beta$ -catenin signalling pathways at different times following SmoM2 expression in  $\alpha 6$ HCD34<sup>+</sup> IFE cells, as measured by real time RT-PCR. Bars represent the mean fold of the relative change in mRNA expression and the error bars represent s.e.m. of the different replicates (control (no TAM,  $n=8$ ), three days ( $n=6$ ) and one ( $n=6$ ), four ( $n=4$ ) and ten (BCC,  $n=6$ ) weeks). WT, wild type. **(b–g)** Immunohistochemistry for  $\beta$ -catenin on paraffin sections of E17.5 embryonic epidermis **(b)**, adult wild-type hair follicle **(c)**, wild-type IFE **(d)** and IFE one week after SmoM2 expression **(e)** and in dysplastic **(f)** and BCC **(g)** lesions, showing the absence of nuclear  $\beta$ -catenin in normal tail IFE cells and the accumulation of nuclear  $\beta$ -catenin as early as one week after SmoM2 expression. Arrows and asterisks highlight cells expressing nuclear  $\beta$ -catenin staining in the epidermis and in the dermis respectively. **(h)**  $\beta$ -galactosidase staining of the Wnt BAT-gal reporter activity in control epidermis and four weeks after SmoM2 expression. **(i–k)** Lef1 expression at

different times following SmoM2 oncogene expression. **(i–k)** Immunostaining of Lef1 and  $\beta 4$ -integrin in E17.5 embryonic epidermis **(i)**, in adult wild-type hair follicle **(j)** and in IFE **(k)**. **(l)** Immunostaining of SmoM2 and Lef1 in IFE cells at different times following SmoM2 expression, showing the rapid expression of Lef1 on SmoM2 expression in adult IFE epidermis. **(m)** Transcriptional analysis of Wnt-related genes in FACS-isolated bulge stem cells ( $\alpha 6$ HCD34<sup>+</sup>) expressing SmoM2 one and four weeks after 10 mg TAM administration to K19CREER/Rosa-SmoM2-YFP mice. The error bars represent s.e.m. of the different replicates (control (no TAM,  $n=9$ ) and one ( $n=6$ ) and four ( $n=4$ ) weeks). **(n–p)** Lef1 and SmoM2 immunostaining in tail epidermis six weeks after 10 mg TAM administration to K19CREER/Rosa-SmoM2-YFP mice showing the absence of Lef1 expression within the bulge and outer root sheath **(o)** cells expressing SmoM2, compared with the normal Lef1 expression in dermal papilla and hair matrix **(p)**. Scale bars, 25  $\mu$ m. HG, hair germ; HP, hair placode; DP, dermal papilla; Mx, matrix; HSP, hair shaft progenitors; Bu, bulge.

was observed in some adult IFE cells, and remained detectable in the placode-like dysplastic lesions and at the leading edge of invasive BCC (Fig. 4e–g). Consistently, BAT-gal mice, which express  $\beta$ -galactosidase under the control of Lef/Tcf responsive elements<sup>27</sup>, showed no  $\beta$ -galactosidase-positive cells in wild-type IFE, and some  $\beta$ -galactosidase-positive cells were found in dysplastic lesions following SmoM2 expression (Fig. 4h). Similarly, Lef1 protein was detectable two weeks after TAM administration and was most strongly expressed when SmoM2-expressing IFE cells adopted a placode-like morphology (Fig. 4l). Lef1 expression persisted at the leading edge of more advanced

dysplastic lesions and invasive BCC (Fig. 4l). These data indicate that Wnt/ $\beta$ -catenin signalling is very rapidly activated after SmoM2 expression in adult IFE cells and is maintained in dysplastic lesions and at the leading edge of invasive BCC.

Under physiological conditions, hair follicle bulge stem cells are highly resistant to SmoM2-induced tumorigenesis<sup>5,6</sup>. To investigate the underlying mechanisms of this resistance, we transcriptionally profiled FACS-isolated adult bulge stem cells ( $\alpha 6$ HCD34<sup>+</sup>, Fig. 1a) expressing SmoM2 one and four weeks after TAM administration to K19CREER/Rosa-SmoM2 mice. Microarray and RT-PCR analysis

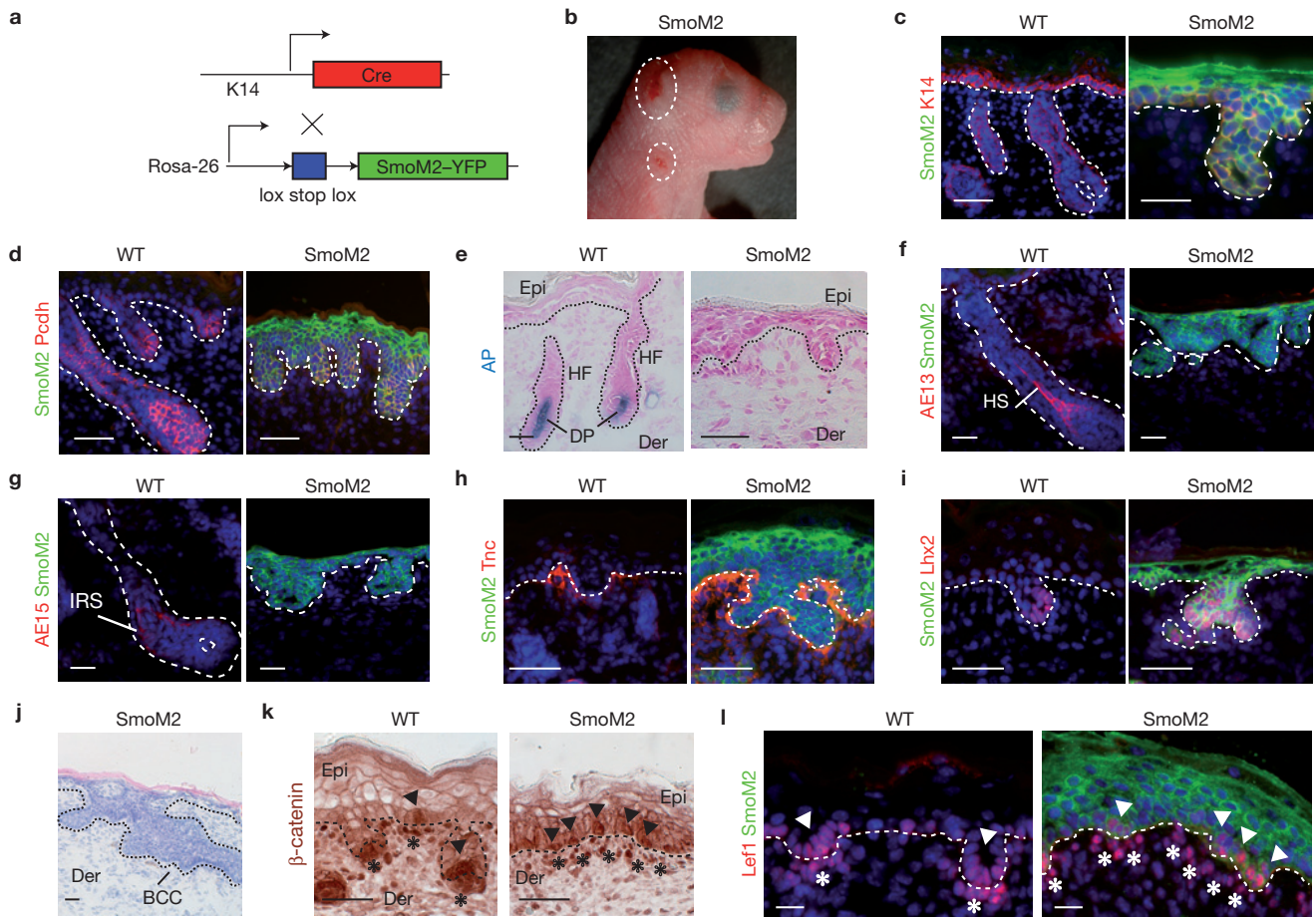


**Figure 5** SmoM2 expression in embryonic epidermis accelerates BCC formation and promotes Wnt/ $\beta$ -catenin signalling activation in the epidermis and its underlying dermis. **(a)** Schematic representation of SmoM2 activation during skin embryonic development using K14CRE recombinase expressed in the early stage of epidermal development. **(b)** Macroscopic picture of K14CRE/Rosa-SmoM2-YFP newborn mouse. The white dots highlight red lesions presented in the neonatal skin of SmoM2-expressing epidermis. **(c,d)** Immunostaining of K14 **(c)** or Pcdh **(d; red)** and SmoM2 (green) in wild-type (WT) and SmoM2-expressing skin epidermis at P1, showing hamartomas that resemble embryonic hair follicles. **(e)** Alkaline phosphatase activity in the wild-type and SmoM2-expressing skin epidermis at P1 demonstrates the absence of dermal papilla cells in SmoM2-expressing epidermis. **(f,g)** Immunostaining of hair follicle terminal differentiation markers AE13 **(f)** or AE15 **(g)** and SmoM2 (green) in wild-type and

SmoM2-expressing epidermis, showing the absence of terminal hair follicle differentiation in SmoM2-expressing cells. **(h,i)** Immunostaining of EHFP markers Tnc **(h)** and Lhx2 **(i)** in wild-type and SmoM2-expressing skin epidermis at P1. **(j)** Haematoxylin and eosin staining of a BCC in SmoM2-expressing epidermis at P1. **(k)** Immunostaining of the  $\beta$ -catenin in wild-type and SmoM2-expressing mice at P1. Arrows and asterisk point nuclear  $\beta$ -catenin staining in the epidermis and the dermis respectively. **(l)** Immunostaining of Lef1 and SmoM2 in wild-type and SmoM2-expressing epidermis at P1. Arrows and asterisks mark the nuclear Lef1 staining in the epidermis and the dermis respectively. Immunostaining of  $\beta$ -catenin and Lef1 shows the cell autonomous (epidermis) and cell nonautonomous (dermis) activation of canonical Wnt signalling on SmoM2 expression in the developing epidermis. Scale bars, 25  $\mu$ m. Der, dermis; DP, dermal papilla; Epi, epidermis; HF, hair follicle; HS, hair shaft; IRS, inner root sheath.

revealed that SmoM2 expression in bulge stem cells upregulated only 21% of the genes found to be upregulated by SmoM2 in IFE cells four weeks after TAM administration (Supplementary Fig. S4a). Although HH signalling is active following SmoM2 expression in bulge stem cells, HH target genes were less upregulated when compared with the IFE cells (Supplementary Fig. S4b). SmoM2 expression in bulge stem cells did not increase the expression of many EHFP signature genes (Supplementary Fig. S4c) and many Wnt pathway components (Fig. 3m). Immunofluorescence analysis showed that Lef1 is not expressed in bulge stem cells six weeks after SmoM2 expression (Fig. 4n, o). These data indicate that SmoM2 expression does not induce Wnt signalling activation and upregulation of EHFP genes in bulge stem cells, probably because of the preferential expression of many negative regulators of Wnt

signalling by bulge stem cells (refs 28,29), which could explain why SmoM2 expression in bulge stem cells does not progress into BCC in their natural environment.

To determine whether concomitant activation of HH and Wnt/ $\beta$ -catenin signalling accelerates BCC initiation, we administered TAM to adult K14CREER/Rosa-SmoM2/ $\beta$ -catenin floxed exon 3 mice<sup>30</sup>, which results in the co-expression of SmoM2 and a truncated, stabilized and constitutively active form of  $\beta$ -catenin. Unexpectedly, this did not accelerate BCC initiation (Supplementary Fig. S5a). The appearance of alkaline phosphatase-positive cells in the dermis following SmoM2 and  $\beta$ -catenin  $\Delta$ exon 3 expression (Supplementary Fig. S5b) indicates that increasing the strength of Wnt signalling in SmoM2-expressing cells may stimulate a differentiation programme that impedes BCC development.

### SmoM2 expression in embryonic epidermis markedly accelerates BCC initiation

To determine whether the observed latency (six to eight weeks) between SmoM2 expression in adult IFE cells and invasive BCC development could result from the progressive embryonic reprogramming of adult IFE cells, we expressed the same level of SmoM2 in the embryonic epidermal progenitors using K14CRE mice, in which the CRE recombinase is expressed in all epidermal cells from the beginning of epidermal development (E12) and thereafter<sup>31</sup> (Fig. 5a). K14CRE/Rosa-SmoM2 mice are born alive but die within 24 h. These mice presented macroscopic red lesions in the skin of the back and ear (Fig. 5b). Microscopic examination confirmed<sup>13,32</sup> that SmoM2 expression in the epidermis during embryonic development induced evenly spaced cellular downgrowths called follicular hamartomas, which resemble embryonic hair follicles, throughout the back skin (Fig. 5c,d). Unlike wild-type hair follicles, these cellular downgrowths were not accompanied by dermal papilla in the dermis, as shown by the absence of alkaline phosphatase-positive cells, and did not present signs of terminal hair follicle differentiation (Fig. 5e–g). Furthermore, invasive BCC was already present in the newborn epidermis (Fig. 5h–j), similar to the malignant lesions found several weeks following oncogene activation in the adult IFE, demonstrating that SmoM2 expression in embryonic epidermal progenitors markedly accelerates BCC development.

In contrast to adult IFE, Wnt/ $\beta$ -catenin signalling activity is high during skin embryonic development, as shown by the higher frequency of cells expressing nuclear  $\beta$ -catenin and Lef1 in the hair follicle, the epidermis and the underlying mesenchyme (Fig. 4k,l), which increased following SmoM2 expression in embryonic epidermis (Fig. 4k,l). These data show that SmoM2 expression in the embryonic epidermis activates Wnt/ $\beta$ -catenin signalling in a cell-autonomous (epidermis) and a non-cell-autonomous (mesenchyme) manner.

### Cell-autonomous role of Wnt/ $\beta$ -catenin during embryonic reprogramming of adult epidermis and tumour initiation mediated by SmoM2

The Wnt/ $\beta$ -catenin pathway is important during embryonic hair follicle development in both epithelial and mesenchymal cells<sup>33–35</sup>. Dkk1 overexpression suppresses tumour formation following SmoM2 expression during embryonic development and thereafter, suggesting that Wnt signalling is required for SmoM2-induced tumour development in the embryonic epidermis by a cell- and/or a non-cell-autonomous mechanism<sup>13</sup>. It remains unclear whether Wnt/ $\beta$ -catenin also controls BCC development in the adult epidermis, and if so at which stages of tumorigenesis, whether it acts in a cell- or in a non-cell-autonomous manner, and what genes  $\beta$ -catenin regulates in this adult oncogenic context.

We simultaneously induced the expression of SmoM2 and the deletion of  $\beta$ -catenin in the adult epidermis and examined the functional consequences of these genetic modifications for the transcriptional programme of oncogene-targeted IFE cells (Supplementary Fig. S6a,b). Administration of 15 mg TAM to K14CREER/Rosa-SmoM2/ $\beta$ -catenin flox/flox (ref. 33) mice resulted in  $\beta$ -catenin deletion and SmoM2 expression in most adult IFE (Supplementary Fig. S6c,d). Absence of  $\beta$ -catenin was not synthetic lethal with oncogenic SmoM2, as demonstrated by the presence of

Smo-YFP-positive cells that are deficient for  $\beta$ -catenin four weeks after TAM administration (Supplementary Fig. S6d). Transcriptional profiling of SmoM2-YFP/ $\beta$ -catenin null at that point revealed that more than 73% of the genes that were commonly upregulated in both EHFP and adult SmoM2-expressing IFE cells were not upregulated by SmoM2 in the absence of  $\beta$ -catenin (Fig. 6a). In the remaining 27% of the commonly upregulated genes between SmoM2 and the EHFP signature, genes such as *Lhx2*, *Gli1* or *Ptch2* remained upregulated by SmoM2 in the absence of  $\beta$ -catenin but were decreased more than fourfold when compared with SmoM2- and  $\beta$ -catenin-expressing cells (Fig. 6a). GSEA demonstrated that the enrichment of commonly upregulated genes between SmoM2-expressing IFE cells and the EHFP signature was lost on  $\beta$ -catenin deletion, whereas the downregulated genes were less affected (Fig. 6b), suggesting that Wnt/ $\beta$ -catenin signalling positively regulates the expression of the EHFP signature in adult IFE oncogene-expressing cells and that other pathways are also important for the repression of the IFE genes.

Real-time qRT-PCR and immunofluorescence analysis of the Wnt/ $\beta$ -catenin signature revealed that some Wnt pathway components were not upregulated by SmoM2 in the absence of  $\beta$ -catenin (Fig. 6c,d), confirming the ablation of the canonical Wnt/ $\beta$ -catenin signalling and suggesting the presence of an amplification loop within the Wnt signalling pathway (for example by upregulation of Wnt ligands and receptors) in this oncogenic setting. Although SmoM2 expression activated HH signalling in the absence of  $\beta$ -catenin (for example upregulation of *Gli1* and *Ptch2*), the level of activation was decreased (Fig. 6c). These data show the critical role of  $\beta$ -catenin in directly and/or indirectly amplifying HH signalling in response to oncogenic Smo expression in this early stage of BCC progression.

In the absence of  $\beta$ -catenin, SmoM2-expressing IFE cells did not adopt a placode-like morphology or downward growth, but maintained their normal morphology and differentiation (Fig. 6e,f). RT-PCR analysis and immunostaining confirmed the absence of upregulation of EHFP markers and transcription factors controlling HF fate decisions (Fig. 6c,g–i). These data demonstrate the critical cell-autonomous role of  $\beta$ -catenin in the reprogramming of adult IFE cells into an EHFP-like fate following SmoM2 expression.

At this high dose of TAM administration, tumour initiation progressed more rapidly, and after four weeks SmoM2-expressing cells had already formed invasive lesions that invaded the underlying dermis (Fig. 7a,b). However, in the absence of  $\beta$ -catenin, the SmoM2-expressing cells survived in the IFE but did not present signs of BCC transformation (Fig. 7c), demonstrating the critical cell-autonomous role of Wnt/ $\beta$ -catenin during SmoM2-induced tumorigenesis in the adult epidermis.

To determine the effects of inhibiting Wnt signalling on tumour formation, we topically administered Wnt-C59, a soluble Wnt inhibitor, for four weeks after SmoM2 expression in adult K14CREER/Rosa-SmoM2 mice. This decreased the size of dysplasia of SmoM2-expressing cells, many of which still presented normal morphology, in contrast to the untreated mice (Fig. 7d,e), indicating that the pharmacological Wnt inhibitor can prevent or delay SmoM2-dependent BCC initiation.

Activation of  $\beta$ -catenin in the adult epidermis reprogrammes the underlying dermis into an embryonic/neonatal stage<sup>36</sup>. To

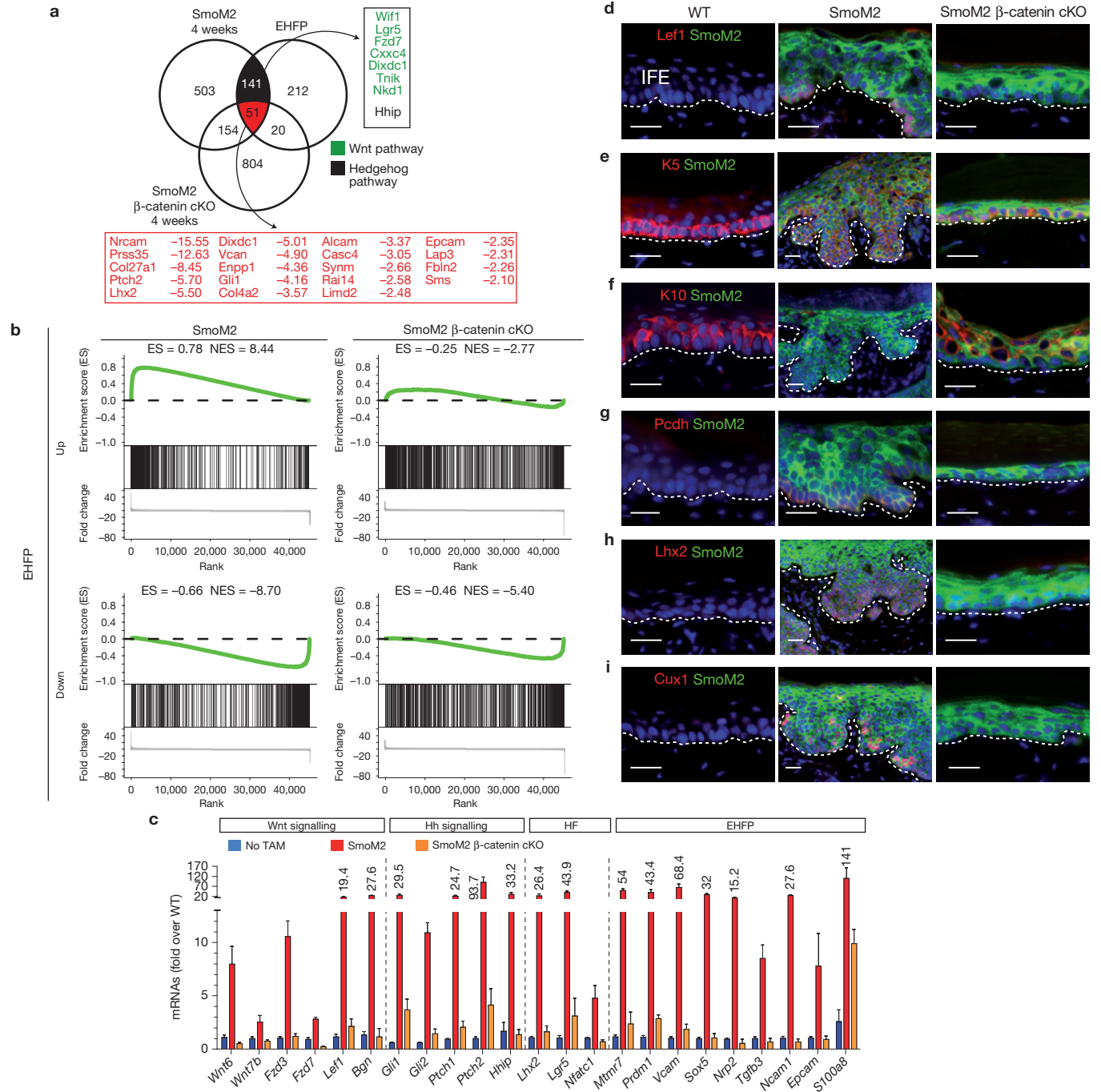


**Figure 6** Cell-autonomous functions of Wnt/ $\beta$ -catenin during SmoM2-induced embryonic hair follicle reprogramming. **(a)** Venn diagrams showing the similarities and the differences between the genes upregulated in the EHFP signature<sup>15</sup> and the genes upregulated by SmoM2 in adult IFE cells ( $\alpha$ 6HCD34<sup>-</sup>) four weeks after SmoM2 expression in the presence and in the absence of  $\beta$ -catenin. The number of common genes between the SmoM2 signature and EHFP signature decreases from 192 to 51 genes. The 141 genes highlighted in black represent the genes lost from the common signature in the absence of  $\beta$ -catenin. The 51 genes highlighted in red represent the genes upregulated by SmoM2 by more than twofold that are still upregulated in the absence of  $\beta$ -catenin. Note the strong downregulation of some of these genes (for example *Lhx2*, *Ptch2* and *Gli1*) following SmoM2 expression in the absence of  $\beta$ -catenin when compared with SmoM2 in the presence of  $\beta$ -catenin (highlighted in red). **(b)** GSEA showing the distribution of the EHFP upregulated (upper) or downregulated (lower) genes within the rank order list of all the microarray probe sets of SmoM2 ( $\alpha$ 6HCD34<sup>-</sup>)

cells four weeks after SmoM2 expression in the presence (left) and in the absence (right) of  $\beta$ -catenin. Note the major decrease of GSEA scores of upregulated genes on  $\beta$ -catenin deletion. The enrichment score (ES) and normalized enrichment score (NES) is shown for each analysis. **(c)** Relative mRNA expression of Wnt/ $\beta$ -catenin signalling-related genes, HH target genes and hair follicle (HF) and EHFP markers in FACS-isolated  $\alpha$ 6HCD34<sup>-</sup> cells from control (no TAM,  $n = 8$ ), from K14CREER/Rosa-SmoM2-YFP mice ( $n = 4$ ) and from K14CREER/Rosa-SmoM2-YFP/ $\beta$ -catenin flox/flox mice ( $n = 5$ ). The bars represent the mean value of relative mRNA expression of different biological replicates and the error bars represent s.e.m. WT, wild type. **(d-i)** Immunostaining of adult wild-type skin and epidermis four weeks after TAM administration to K14CREER/Rosa-SmoM2-YFP mice and to K14CREER/Rosa-SmoM2-YFP/ $\beta$ -catenin flox/flox mice. SmoM2 expression is represented in green, whereas *Lef1* **(d)**, the basal cell marker *K5* **(e)**, the differentiated cell marker *K10* **(f)** and the EHFP and hair follicle markers *Pcdh* **(g)**, *Lhx2* **(h)** and *Cux1* **(i)** are represented in red. Scale bars, 50  $\mu$ m.

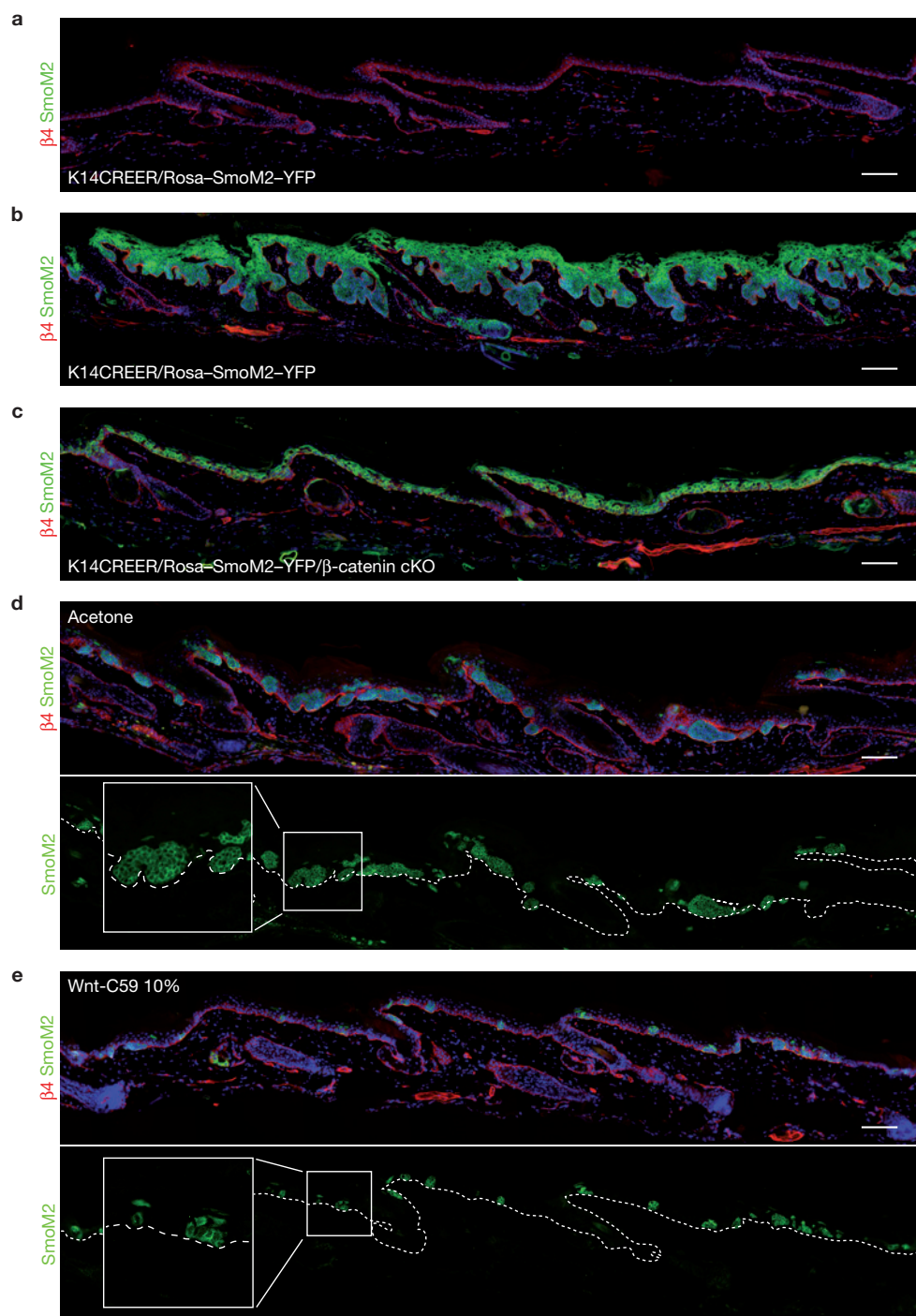


**Figure 7** Cell-autonomous role of Wnt/ $\beta$ -catenin in SmoM2-induced tumorigenesis and pharmacological inhibition of tumour initiation in the adult epidermis. (**a–c**) Immunostaining of SmoM2 (green) and  $\beta$ 4-integrin (red) in tail epidermis in absence of SmoM2 expression (**a**), four weeks after 15 mg TAM administration to K14CREER/Rosa-SmoM2-YFP (**b**) and K14CREER/Rosa-SmoM2-YFP/ $\beta$ -catenin flox/flox (**c**) floxed mice. Note the

absence of tumour initiation following SmoM2 expression in the absence of  $\beta$ -catenin in the adult epidermis. (**d,e**) Immunostaining of  $\beta$ 4-integrin (red) and SmoM2 (green) in K14CREER/Rosa-SmoM2-YFP tail epidermis four weeks after acetone (**d**) and Wnt-C59 (10%) treatment (**e**), showing the smaller size of SmoM2-expressing clones in Wnt-C59 treated mice.  $n = 3$  mice for each group. Scale bars, 100  $\mu$ m.

study whether this also occurs in the dermis of SmoM2-expressing epidermis, we investigated the expression of markers previously associated with such reprogramming. As previously described<sup>36</sup>, Pdgfr- $\alpha$  and Vimentin expression were more enriched in the neonatal epidermis and became mostly restricted to dermal papillae and mesenchymal cells surrounding the lower hair follicle in the adult

skin (Supplementary Fig. S7a,b). SmoM2 induction in the epidermis increased Pdgfr- $\alpha$  and Vimentin expression within the adult dermis surrounding SmoM2-expressing cells (Supplementary Fig. S7c,d). Pdgfr- $\alpha$  presented a more restricted expression at the leading edge of BCC, whereas Vimentin was more diffusely expressed in the dermis. Herovici staining, which discriminates between young (light

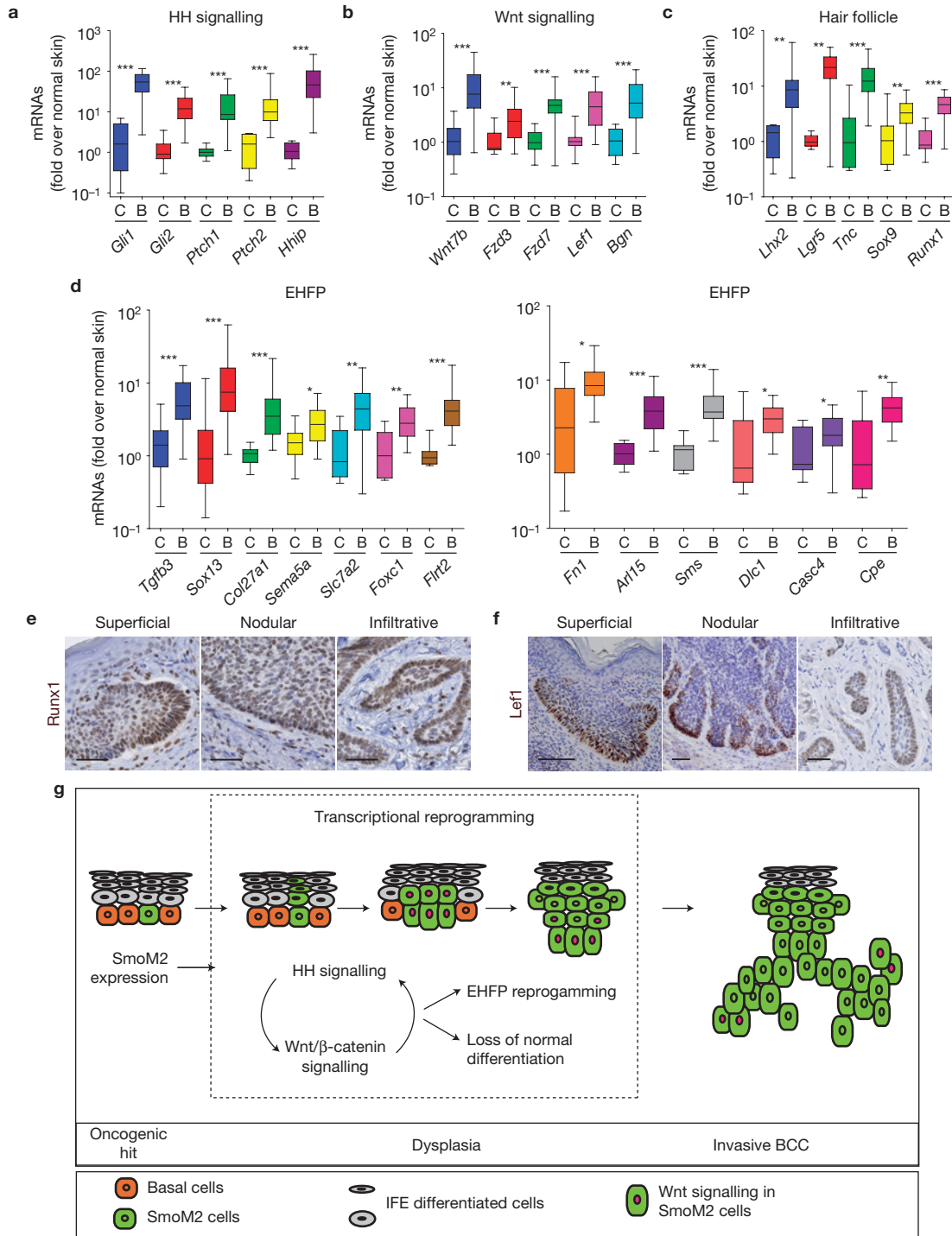


**Figure 8** Human BCCs express markers of the Wnt/β-catenin and EHFP signatures. (a–d) Box-and-whisker diagrams representing the relative gene expression of Hedgehog (HH) signalling (a), Wnt/β-catenin signalling (b), hair follicles (c) and EHFPs (d) in control normal human skin samples (indicated by the letter C,  $n = 10$ ) and in a prospective collection of human BCCs (indicated by the letter B,  $n = 25$ ). Gene expression is normalized to the mean expression of the normal skin samples. In the box-and-whisker diagrams, the boxes represent the quartiles of the data and the whiskers represent the minimal and the maximal values of the series. Statistical analyses were carried out using a Mann–Whitney test ( $*P < 0.05$ ,  $**P < 0.01$ ,  $***P < 0.001$ ). (e,f) Immunostaining of EHFP marker Runx1 (e) and Wnt/β-catenin transcription factor Lef1

(f). Note the enrichment of Runx1 and Lef1 expression at the leading edge of the tumours. Scale bars, 50 μm. (g) Model summarizing the mechanisms regulating the early step of BCC initiation. SmoM2 expression in tumour-initiating cells leads to a rapid and profound change in gene expression that induces a fate change in IFE progenitors, which stop to differentiate into suprabasal cornified cells and acquire a morphology and a gene expression profile presenting striking similarities with normal EHFPs before progressing into invasive carcinoma. SmoM2 expression in adult IFE cells rapidly activates the Wnt/β-catenin signalling pathway, which in turn regulates the embryonic hair follicle reprogramming of adult IFE cells and sustains HH signalling in a positive feedback loop to initiate BCC development.

blue) and mature collagen fibres (pink), shows light blue staining within the dermis underlying SmoM2-expressing epidermis and surrounding dysplasia and BCC (Supplementary Fig. S7e). These data indicate that dermal cells also undergo reprogramming into a more embryonic/neonatal stage following SmoM2 expression in the epidermis, suggesting crosstalk between SmoM2-expressing cells and their underlying mesenchyme, which probably plays an important role in BCC initiation.

### Human BCC presents upregulation of the Wnt/ $\beta$ -catenin and EHFP signatures.

Human BCCs are very heterogeneous and are classified into different histological subtypes, with superficial, nodular and infiltrative BCCs being among the most common ones<sup>37</sup>. Human BCCs express hair follicle markers<sup>7–13</sup> and present signs of  $\beta$ -catenin signalling activity<sup>38–40</sup>. To investigate whether these lesions are also reprogrammed into an EHFP-like state and express the same EHFP and Wnt signatures as found in the mouse BCCs, we determined the levels of HH, EHFP and the Wnt/ $\beta$ -catenin gene signatures on a prospective cohort of patients presenting clinical signs of BCC. mRNA obtained from 25 different BCCs confirmed by independent pathological examination was used to compare the expression of various EHFP, HH and Wnt markers with 10 control skin biopsies taken from the same anatomical sites as the tumours. As expected, human BCCs massively upregulated the expression of HH target genes (for example *Gli1/2*, *Ptch1/2* and *Hhip*; Fig. 8a), with most of the human BCCs upregulating the Wnt signalling signature found in our mouse model (for example upregulation of *Wnt7b*, *Fzd3*, *Fzd7*, *Lef1* and *Biglycan*; Fig. 8b). The majority of primary BCCs, irrespective of their histology, present a strong upregulation of previously described adult and embryonic hair follicle markers (for example *Sox9*, *Lgr5*; refs 10–12), as well as many other hair follicle markers including *Lhx2* (ref. 15) and *Runx1* (refs 17,18; Fig. 8c) and markers more specifically enriched in EHFPs (ref. 15), such as *Tgf- $\beta$ 3*, *Sox13*, *Col27a1* or *Foxc1* (Fig. 8d).

Immunohistochemistry on 15 primary human BCCs from different subtypes (five superficial, five nodular and five infiltrative BCCs) revealed that the EHFP markers *Runx1*, *Cux1* and *Edar* were preferentially enriched at the leading edge of the majority of human BCCs irrespective of their histological subtypes, although the level of expression and the percentage of BCC cells expressing these markers varied between patients, with lower expression in the infiltrative BCC subtype (Fig. 8e and Supplementary Fig. S8a–c and Table S2). Immunohistochemical analysis also showed the expression of nuclear  $\beta$ -catenin in most human BCCs and the preferential expression of *Lef1* at the tumours' leading edges (Supplementary Fig. S8d, Fig. 8f and Supplementary Table S2), demonstrating that activation of the Wnt/ $\beta$ -catenin signalling pathway and *Lef1* expression are hallmarks of human BCCs of all histological subtypes.

### DISCUSSION

By prospectively isolating BCC-initiating cells and carrying out transcriptional profiling at different stages of tumour initiation in adult mice, we have demonstrated that adult IFE cells expressing SmoM2 undergo rapid transcriptional reprogramming into an EHFP-like fate before progressing into invasive carcinoma. Although the concept

that cancer cells can be reprogrammed into a more primitive fate has long been suggested, no whole genome transcriptional approach had so far addressed this question quantitatively and systematically. Using such an approach, genes belonging to the pluripotent embryonic stem cell signature were shown to be overexpressed in cancer<sup>41,42</sup>, which was proposed to be due to an upregulation of Myc-controlled genes rather than through direct regulation of the core pluripotency network<sup>43</sup>. Although our data revealed that adult IFE progenitors are indeed reprogrammed into a more embryonic-like hair follicle progenitor state, oncogenic Smo did not induce the expression of pluripotency network genes. Instead, oncogenic Smo expression in adult IFE cells induced transcriptional reprogramming into an EHFP-like fate, already detectable at the mRNA level less than a week after oncogene expression and strongly suggesting that these rapid changes are transcriptionally or epigenetically regulated rather than resulting from genetic mutations.

Overexpression of *Dkk1* was shown to inhibit tumour formation after SmoM2 expression in the embryonic epidermis, suggesting that Wnt signalling is required for tumorigenesis in this embryonic context<sup>13</sup>. We demonstrate that the activation of Wnt/ $\beta$ -catenin signalling pathways is one of the earliest molecular changes associated with oncogenic Smo expression in the adult IFE and that it persists at the leading edge of invasive tumours. Genetic loss of  $\beta$ -catenin together with SmoM2 expression showed that Wnt/ $\beta$ -catenin signalling is required in a cell-autonomous manner for the reprogramming of adult IFE progenitors into EHFP-like fate as well as for tumour initiation. Our data also indicate that pharmacological inhibition of Wnt signalling can prevent or delay tumour initiation. Further studies will determine whether this approach can be clinically effective against tumour progression.

Different feedback mechanisms between HH and Wnt signalling are known during embryonic and tumour development. In the normal epidermis, Wnt signalling acts genetically upstream of HH during hair follicle specification, *de novo* hair follicle formation and activation of adult hair follicle stem cells<sup>33,44–46</sup>, and Shh signalling is not required for Wnt/ $\beta$ -catenin activation<sup>45</sup>. In contrast, our studies revealed that  $\beta$ -catenin acts downstream of oncogenic HH signalling but is also necessary to sustain HH signalling in response to SmoM2, as well as in amplifying Wnt/ $\beta$ -catenin signalling itself by a cell-autonomous mechanism. Although future studies will fully elucidate the molecular mechanisms underlying these genetic interactions, our results demonstrate that  $\beta$ -catenin controls an amplification loop that sustains Wnt and HH signalling, which cooperate for the reprogramming of adult tumour-initiating cells into EHFP-like cells and BCC initiation (Fig. 8g).

Human BCCs express markers of both adult hair follicle stem cells and EHFPs (refs 7–12,47,48), but whether this is more representative of embryonic or adult state was unclear. We reveal that the EHFP signature found in the BCC mouse model is also upregulated in all human BCC subtypes. Moreover, although human BCCs present signs of canonical Wnt/ $\beta$ -catenin activation and *Lef1* expression<sup>38–40</sup>, our analysis shows that a Wnt signature composed of a particular set of Wnt ligands, receptors, transcription factors and target genes is upregulated in both mouse and human BCCs irrespective of their histological subtypes, which could represent interesting candidates for pharmacological inhibition. □

## METHODS

Methods and any associated references are available in the online version of the paper.

*Note: Supplementary Information is available in the online version of the paper*

## ACKNOWLEDGEMENTS

We would like to thank those who provided us with reagents and who are acknowledged in the text. C.B. is an investigator of WELBIO. C.B. is a *chercheur qualifié*, S.B. is a *chargé de recherche* and G.L. is a *collaborateur scientifique* of the FRS/FNRS; K.K.Y. is supported by TELEVIE. This work was supported by the FNRS, the *program d'excellence* CIBLES of the Wallonia Region, a research grant from the Fondation Contre le Cancer, the Fondation ULB, the Fond Yvonne Boël and the Fond Gaston Ithier, a starting grant of the European Research Council (ERC) and the EMBO Young Investigator Program.

## AUTHOR CONTRIBUTIONS

C.B. and K.K.Y. designed the experiments and carried out the data analysis; K.K.Y., G.L., K.B., O.A., J.C.L., V.S., B.V.S., S.D., S.A. and D.P. carried out most of the experiments; S.B. carried out bioinformatic analysis of the microarray; S.R. and I.S. carried out immunohistochemistry analysis on human BCCs; J.V.B. and V.D.M. provided human biopsy materials; C.B. and K.K.Y. wrote the manuscript.

## COMPETING FINANCIAL INTERESTS

The authors declare no competing financial interests.

Published online at [www.nature.com/doi/10.1038/ncb2628](http://www.nature.com/doi/10.1038/ncb2628)

Reprints and permissions information is available online at [www.nature.com/reprints](http://www.nature.com/reprints)

- Epstein, E. H. Basal cell carcinomas: attack of the hedgehog. *Nat. Rev. Cancer* **8**, 743–754 (2008).
- Pasca di Magliano, M. & Hebrok, M. Hedgehog signalling in cancer formation and maintenance. *Nat. Rev. Cancer* **3**, 903–911 (2003).
- Xie, J. *et al.* Activating Smoothed mutations in sporadic basal-cell carcinoma. *Nature* **391**, 90–92 (1998).
- Mao, J. *et al.* A novel somatic mouse model to survey tumorigenic potential applied to the Hedgehog pathway. *Cancer Res.* **66**, 10171–10178 (2006).
- Youssef, K. K. *et al.* Identification of the cell lineage at the origin of basal cell carcinoma. *Nat. Cell Biol.* **12**, 299–305 (2010).
- Wong, S. Y. & Reiter, J. F. Wounding mobilizes hair follicle stem cells to form tumors. *Proc. Natl Acad. Sci. USA* **108**, 4093–4098 (2011).
- Shirahama, S., Furukawa, F., Wakita, H. & Takigawa, M. E- and P-cadherin expression in tumor tissues and soluble E-cadherin levels in sera of patients with skin cancer. *J. Dermatol. Sci.* **13**, 30–36 (1996).
- Yoshikawa, K., Katagata, Y. & Kondo, S. Biochemical and immunohistochemical analyses of keratin expression in basal cell carcinoma. *J. Dermatol. Sci.* **17**, 15–23 (1998).
- Markey, A. C., Lane, E. B., Macdonald, D. M. & Leigh, I. M. Keratin expression in basal cell carcinomas. *Br. J. Dermatol.* **126**, 154–160 (1992).
- Vidal, V. P. *et al.* Sox9 is essential for outer root sheath differentiation and the formation of the hair stem cell compartment. *Curr. Biol.* **15**, 1340–1351 (2005).
- Vidal, V. P., Ortonne, N. & Schedl, A. SOX9 expression is a general marker of basal cell carcinoma and adnexal-related neoplasms. *J. Cutan. Pathol.* **35**, 373–379 (2008).
- Tanese, K. *et al.* G-protein-coupled receptor GPR49 is up-regulated in basal cell carcinoma and promotes cell proliferation and tumor formation. *Am. J. Pathol.* **173**, 835–843 (2008).
- Yang, S. H. *et al.* Pathological responses to oncogenic Hedgehog signaling in skin are dependent on canonical Wnt/ $\beta$ -catenin signaling. *Nat. Genet.* **40**, 1130–1135 (2008).
- Bianpain, C., Lowry, W. E., Geoghegan, A., Polak, L. & Fuchs, E. Self-renewal, multipotency, and the existence of two cell populations within an epithelial stem cell niche. *Cell* **118**, 635–648 (2004).
- Rhee, H., Polak, L. & Fuchs, E. Lhx2 maintains stem cell character in hair follicles. *Science* **312**, 1946–1949 (2006).
- Subramanian, A. *et al.* Gene set enrichment analysis: a knowledge-based approach for interpreting genome-wide expression profiles. *Proc. Natl Acad. Sci. USA* **102**, 15545–15550 (2005).
- Osorio, K. M. *et al.* Runx1 modulates developmental, but not injury-driven, hair follicle stem cell activation. *Development* **135**, 1059–1068 (2008).
- Osorio, K. M., Lilja, K. C. & Tumber, T. Runx1 modulates adult hair follicle stem cell emergence and maintenance from distinct embryonic skin compartments. *J. Cell Biol.* **193**, 235–250 (2011).
- Ellis, T. *et al.* The transcriptional repressor CDP (Cutl1) is essential for epithelial cell differentiation of the lung and the hair follicle. *Genes Dev.* **15**, 2307–2319 (2001).
- Wang, G. Y., Wang, J., Mancianti, M. L. & Epstein, E. H. Jr Basal cell carcinomas arise from hair follicle stem cells in Ptch1(+/-) mice. *Cancer Cell* **19**, 114–124 (2011).
- Kasper, M. *et al.* Wounding enhances epidermal tumorigenesis by recruiting hair follicle keratinocytes. *Proc. Natl Acad. Sci. USA* **108**, 4099–4104 (2011).
- Uhmann, A. *et al.* The Hedgehog receptor Patched controls lymphoid lineage commitment. *Blood* **110**, 1814–1823 (2007).
- Lowry, W. E. *et al.* Defining the impact of  $\beta$ -catenin/Tcf transactivation on epithelial stem cells. *Genes Dev.* **19**, 1596–1611 (2005).
- DasGupta, R. & Fuchs, E. Multiple roles for activated LEF/TCF transcription complexes during hair follicle development and differentiation. *Development* **126**, 4557–4568 (1999).
- Enshell-Seiffers, D., Lindon, C., Kashiwagi, M. & Morgan, B. A.  $\beta$ -catenin activity in the dermal papilla regulates morphogenesis and regeneration of hair. *Dev. Cell* **18**, 633–642 (2010).
26. Rendl, M., Lewis, L. & Fuchs, E. Molecular dissection of mesenchymal-epithelial interactions in the hair follicle. *PLoS Biol.* **3**, e331 (2005).
- Maretto, S. *et al.* Mapping Wnt/ $\beta$ -catenin signaling during mouse development and in colorectal tumors. *Proc. Natl Acad. Sci. USA* **100**, 3299–3304 (2003).
- Tumber, T. *et al.* Defining the epithelial stem cell niche in skin. *Science* **303**, 359–363 (2004).
- Morris, R. J. *et al.* Capturing and profiling adult hair follicle stem cells. *Nat. Biotechnol.* **22**, 411–417 (2004).
- Harada, N. *et al.* Intestinal polyposis in mice with a dominant stable mutation of the  $\beta$ -catenin gene. *EMBO J.* **18**, 5931–5942 (1999).
- Vasioukhin, V., Bauer, C., Degenstein, L., Wise, B. & Fuchs, E. Hyperproliferation and defects in epithelial polarity upon conditional ablation of  $\alpha$ -catenin in skin. *Cell* **104**, 605–617 (2001).
- Grachtchouk, V. *et al.* The magnitude of hedgehog signaling activity defines skin tumor phenotype. *EMBO J.* **22**, 2741–2751 (2003).
- Huelsken, J., Vogel, R., Erdmann, B., Cotsarelis, G. & Birchmeier, W.  $\beta$ -Catenin controls hair follicle morphogenesis and stem cell differentiation in the skin. *Cell* **105**, 533–545 (2001).
- Andl, T., Reddy, S. T., Gaddapara, T. & Millar, S. E. WNT signals are required for the initiation of hair follicle development. *Dev. Cell* **2**, 643–653 (2002).
- Enshell-Seiffers, D., Lindon, C., Wu, E., Takeo, M. M. & Morgan, B. A.  $\beta$ -catenin activity in the dermal papilla of the hair follicle regulates pigment-type switching. *Proc. Natl Acad. Sci. USA* **107**, 21564–21569 (2010).
- Collins, C. A., Kretzschmar, K. & Watt, F. M. Reprogramming adult dermis to a neonatal state through epidermal activation of  $\beta$ -catenin. *Development* **138**, 5189–5199 (2011).
- Crowson, A. N. Basal cell carcinoma: biology, morphology and clinical implications. *Mod. Pathol.* **19** (Suppl 2), S127–S147 (2006).
- El-Bahrawy, M., El-Masry, N., Alison, M., Poulson, R. & Fallowfield, M. Expression of  $\beta$ -catenin in basal cell carcinoma. *Br. J. Dermatol.* **148**, 964–970 (2003).
- Saldanha, G., Ghura, V., Potter, L. & Fletcher, A. Nuclear  $\beta$ -catenin in basal cell carcinoma correlates with increased proliferation. *Br. J. Dermatol.* **151**, 157–164 (2004).
- Kriegel, L., Horst, D., Kirchner, T. & Jung, A. LEF-1 expression in basal cell carcinomas. *Br. J. Dermatol.* **160**, 1353–1356 (2009).
- Wong, D. J. *et al.* Module map of stem cell genes guides creation of epithelial cancer stem cells. *Cell Stem Cell* **2**, 333–344 (2008).
- Ben-Porath, I. *et al.* An embryonic stem cell-like gene expression signature in poorly differentiated aggressive human tumors. *Nat. Genet.* **40**, 499–507 (2008).
- Kim, J. *et al.* A Myc network accounts for similarities between embryonic stem and cancer cell transcription programs. *Cell* **143**, 313–324 (2010).
- Gat, U., DasGupta, R., Degenstein, L. & Fuchs, E. De Novo hair follicle morphogenesis and hair tumors in mice expressing a truncated  $\beta$ -catenin in skin. *Cell* **95**, 605–614 (1998).
- St-Jacques, B. *et al.* Sonic hedgehog signaling is essential for hair development. *Curr. Biol.* **8**, 1058–1068 (1998).
- Silva-Vargas, V. *et al.*  $\beta$ -catenin and Hedgehog signal strength can specify number and location of hair follicles in adult epidermis without recruitment of bulge stem cells. *Dev. Cell* **9**, 121–131 (2005).
- Zhang, Y. *et al.* Activation of  $\beta$ -catenin signaling programs embryonic epidermis to hair follicle fate. *Development* **135**, 2161–2172 (2008).
- Krahl, D. & Sellheyer, K. Basal cell carcinoma and pilomatixoma mirror human follicular embryogenesis as reflected by their differential expression patterns of SOX9 and  $\beta$ -catenin. *Br. J. Dermatol.* **162**, 1294–1301 (2010).

## METHODS

**Animals.** K14CRE transgenic mice<sup>29</sup> and K14CREER transgenic mice<sup>49</sup> were kindly provided by Elaine Fuchs, The Rockefeller University. The K19CREER knock-in mice<sup>50</sup> were kindly provided by Guoqiang Gu, The Vanderbilt University Medical Center. P $\beta$ 1 flox/flox mice and Rosa–SmoM2–YFP mice<sup>3</sup> were obtained from the JAX repository.  $\beta$ -catenin flox/flox (ref. 31),  $\beta$ -catenin floxed exon 3 (ref. 28) and BAT-gal reporter mice<sup>27</sup> were kindly provided respectively by Walter Birchmeier, Max Delbrück Center for Molecular Medicine, M. M. Taketo, Kyoto University, and Stefano Piccolo, University of Padua. Mouse colonies were maintained in a certified animal facility in accordance with European guidelines. Female and male animals have been used for all experiments and equal animal gender ratios have been respected in the majority of the analysis.

**Targeting oncogene activation.** For clonal induction—K14CREER/Rosa–SmoM2–YFP mice were treated at D28 with 1 mg of tamoxifen (Sigma-Aldrich) by intraperitoneal injection and analysed one, four or ten weeks after tamoxifen administration.

For high level of recombination to ensure deletion of  $\beta$ -catenin or stabilized  $\beta$ -catenin expression together with SmoM2 expression—one-month-old K14CREER/Rosa–SmoM2–YFP, K14CREER/Rosa–SmoM2–YFP/ $\beta$ -catenin flox/flox and K14CREER/Rosa–SmoM2–YFP/ $\beta$ -catenin floxed exon 3 mice were treated with  $6 \times 2.5$  mg of tamoxifen by intraperitoneal injection.

For P $\beta$ 1 loss of function—K14CREER/P $\beta$ 1 flox/flox mice were treated at D28 with 1 mg of tamoxifen by intraperitoneal injection and analysed four or nine weeks after tamoxifen administration.

For bulge stem cell targeting—one-month-old K19CREERT2/Rosa–SmoM2–YFP mice were treated with  $4 \times 2.5$  mg of tamoxifen by intraperitoneal injection.

**Histology, immunostaining and imaging.** For all adult studies, the tail and paw skin were embedded in optimal cutting temperature compound (OCT, Sakura) and cut into 5–8  $\mu$ m frozen sections using a CM3050S Leica cryostat (Leica Microsystems) and a Microm HM60 cryostat. For paraffin sections, tissues were prefixed for 24 h with 4% paraformaldehyde at 4 °C before embedding.

For embryonic studies, entire mice embryos were embedded at E17 in OCT and cut into 5–8  $\mu$ m frozen sections using a CM3050S Leica cryostat.

Immunostainings were carried out on frozen sections. Owing to the fusion of SmoM2 with YFP, SmoM2-expressing cells were detected using anti-GFP antibody.

Frozen sections were dried and then fixed with 4% paraformaldehyde/PBS for 10 min at room temperature and blocked with a blocking buffer for 1 h (PBS, horse serum 5%, BSA 1%, Triton 0.1–0.2%). Skin sections were incubated with primary antibodies diluted in blocking buffer overnight at 4 °C, washed with PBS for 3  $\times$  5 min, and then incubated with Hoechst solution and secondary antibodies diluted in blocking buffer for 1 h at room temperature. Finally, sections were washed with PBS for 3  $\times$  5 min at room temperature and mounted. For mouse monoclonal antibodies, immunostainings were carried out following the MOM kit's instructions. The lists of primary and secondary antibodies are shown in Supplementary Table S4. All pictures of immunostaining were acquired using an Axio Imager M1 microscope, an AxioCamMR3 or MrC5 camera and the Axiovision software (Carl Zeiss).

**$\beta$ -catenin immunohistochemistry.** Paraffin sections were used to detect nuclear  $\beta$ -catenin expression. After deparaffinization and rehydration, sections were incubated in PBS with 0.5% Triton for 15 min and the antigen unmasking procedure was carried out for 30 min at 98 °C in citrate buffer/Tween 0.1% at pH 6 using a PT Module (Lab Vision). Endogenous peroxidase was blocked using 3% H<sub>2</sub>O<sub>2</sub> (Merck) in methanol (VWR) for 10 min at room temperature. Endogenous avidin and biotin were blocked using an Endogenous Blocking Kit (Invitrogen) for 20 min at room temperature. Non-specific antigen blocking was carried out using MOM Basic Kit reagent supplemented with Triton 0.3%. Mouse anti- $\beta$ -catenin (1/1,000, Abcam, clone 15b8, ab6301) was incubated overnight at 4 °C. Anti-mouse biotinylated antibody provided in the MOM blocking kit and Standard ABC Kit and ImmPACT DAB (Vector Laboratories) were used for horseradish peroxidase activity.

**Alkaline phosphatase staining.** The used protocol was carried out following the manufacturer's instructions (Roche). Nuclei were counterstained with nuclear fast red solution for 15 min and sections washed twice in PBS. Sections were dehydrated and were mounted in Safe Mount.

**X-gal staining.** Tails from BAT-gal mice were prefixed for 15 min with 4% paraformaldehyde, washed in PBS and then incubated at 37 °C for 24 h in X-gal solution (5-bromo-4-chloro-3-indoyl- $\beta$ -D-galactoside (1 mg; Sigma-Aldrich), potassium ferricyanide crystalline (5 mM), potassium ferricyanide trihydrate (5 mM), magnesium chloride (2 mM), deoxycholate 0.05%, NP-40 0.02%, in PBS). After washing in PBS, tail tissues were embedded in OCT.

**Herovici staining.** Paraffin sections were used and the Herovici staining was carried out as previously described<sup>36</sup>.

**Isolation of keratinocytes and RNA extraction.** Tail skins were separated from the tail bone and incubated overnight in trypsin at 4 °C (Gibco). The next day the epidermis was separated from the dermis and incubated for 20 min in trypsin on a rocking plate. Trypsin was neutralized by adding DMEM containing 10% Chelex serum. The cell suspension was then passed twice through a 40  $\mu$ m cell strainer.

After isolation of keratinocytes, immunostaining was carried out using Alexa647-conjugated anti-CD34 (clone RAM34; BD Biosciences) and PE-conjugated anti- $\alpha$ 6-integrin (clone GoH3; BD biosciences) as described<sup>15</sup>. After doublet exclusion, living SmoM2-expressing epidermal cells were gated by forward scatter, by side scatter and by negative staining for Hoechst and by expression of SmoM2–YFP. Fluorescence-activated cell-sorting analysis was carried out using FACSAria and FACSDiva software (BD Biosciences). For microarray analysis, sorted cells were harvested directly in the lysis buffer provided by the manufacturer (microprep kit, RNaseasy, Stratagen) and RNA extraction was then carried out according to the manufacturer's protocol.

**RT–PCR analysis of human BCCs.** BCC tissues were obtained from 25 patients with pathological confirmed BCCs using punch biopsy materials after informed consent, and normal skin was obtained from ten patients undergoing wound reconstruction (protocol ID P2009/313). Each sample from tumour or normal skin was directly frozen in liquid nitrogen and stored at –80 °C.

Each sample was first reduced in powder using mortar frozen by liquid nitrogen and digested in TRIzol using a homogenizer machine. RNA phase was extracted after chloroform addition and precipitated with 70% ethanol. A MiniRNeasy kit (Qiagen) was used to purify RNA following the manufacturer's instructions.

**Reverse transcription and quantitative real-time PCR.** Each RNA was quantified using a NanoDrop spectrophotometer. Purified RNA was used to synthesize the first-strand complementary DNA using SuperScript II (Invitrogen) with random hexamers (Roche). Quantitative PCR analyses were carried out with 1 or 2 ng of cDNA as template, using a Brilliant II Fast SYBR QPCR Master Green mix (Stratagen) and an Agilent Technologies Stratagene Mx3500P real-time PCR system.

All primers were designed using Lasergene 7.2 software (DNASTAR) or the Assay Design Center (Roche Applied Science, [https://www.roche-applied-science.com/sis/rtqcr/upl/index.jsp?id=uplct\\_030000](https://www.roche-applied-science.com/sis/rtqcr/upl/index.jsp?id=uplct_030000)). The lists of primers are shown in Supplementary Tables S5 and S6.

Analysis of results was carried out with MxPro software (Stratagene). Delta delta CT was used to calculate the relative expression to the control samples using the housekeeping genes ubiquitin C (UBC) for human samples and *Tbp* for mouse samples.

**Microarray analysis.** Total RNAs were isolated from sorted cells and were labelled and hybridized on a mouse genome 430 2.0 array. Microarrays were carried out in triplicate for the K14CREER/Rosa–SmoM2–YFP sorted cells and in duplicate for the K14CREER/Rosa–SmoM2–YFP/ $\beta$ -catenin flox/flox. All the results were normalized using the frozen robust multiarray analysis normalization using the R/Bioconductor package *fRMA* (refs 51,52) with standard parameters. Genetic signatures were obtained by considering genes presenting a fold change greater or smaller than 2 or –2 respectively. The hypergeometric *P*-value indicates the probability of observing by chance the same overlap between the query set and the reference set.

**Gene set enrichment analysis (GSEA).** The GSEA program was downloaded from the BROAD institute website (<http://www.broadinstitute.org/gsea/>). We used the GSEA *preranked* option with standard parameters of weighted enrichment score calculation to run the GSEA against a user-supplied fold-change-ranked list of genes. Results of the enrichment analysis were plotted using R software.

**Microarray data access.** The primary data discussed in this publication have been deposited in the NCBI Gene Expression Omnibus and are accessible through GEO series accession number GSE40612. <http://www.ncbi.nlm.nih.gov/geo/query/acc.cgi?acc=GSE40612>.

The bulge stem cell signature<sup>14</sup> is accessible through GEO series accession number GSE41704. <http://www.ncbi.nlm.nih.gov/geo/query/acc.cgi?acc=GSE41704>.

- Vasioukhin, V., Degenstein, L., Wise, B. & Fuchs, E. The magical touch: genome targeting in epidermal stem cells induced by tamoxifen application to mouse skin. *Proc. Natl Acad. Sci. USA* **96**, 8551–8556 (1999).
- Means, A. L., Xu, Y., Zhao, A., Ray, K. C. & Gu, G. A CK19(CreERT) knockin mouse line allows for conditional DNA recombination in epithelial cells in multiple endodermal organs. *Genesis* **46**, 318–323 (2008).
- Gentleman, R. C. *et al.* Bioconductor: open software development for computational biology and bioinformatics. *Genome Biol.* **5**, R80 (2004).
- McCall, M. N., Bolstad, B. M. & Irizarry, R. A. Frozen robust multiarray analysis (*fRMA*). *Biostatistics* **11**, 242–253 (2010).

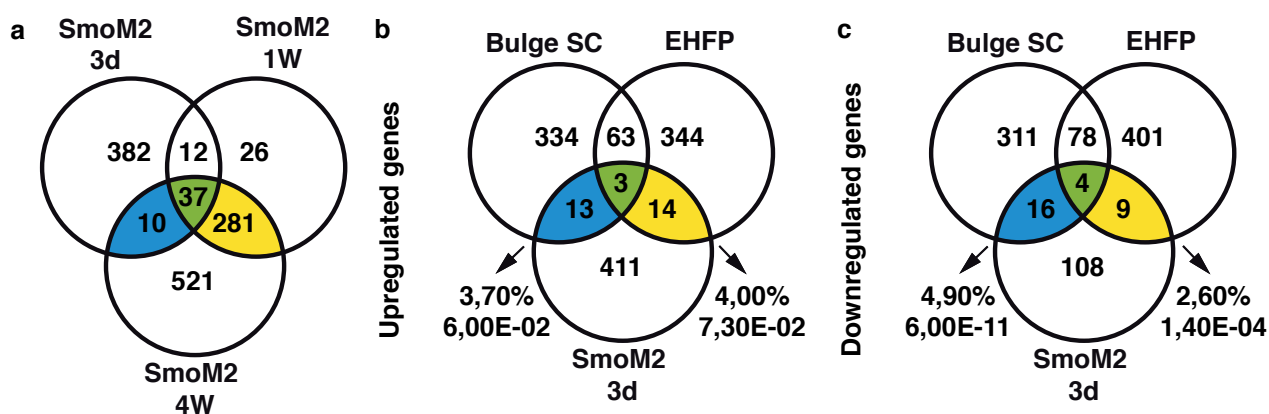


**Figure S1** Transcriptional analysis of FACS isolated IFE cells 3 days following SmoM2 expression. (a) Venn diagrams showing the similarities and the differences between the number of upregulated genes differentially regulated by SmoM2 in adult IFE cells 3 days, 1 week and 4 Weeks after SmoM2 expression in a6HCD34- cells. (b-c) Venn diagrams showing the

similarities and the differences between the genes differentially upregulated genes (b) or downregulated genes (c) 3 days after TAM administration, with the EHFP and adult bulge SC signature. Arrows indicate the percentage and the hypergeometric P-value of the overlap between SmoM2 signature and EHFP or bulge SC signature.

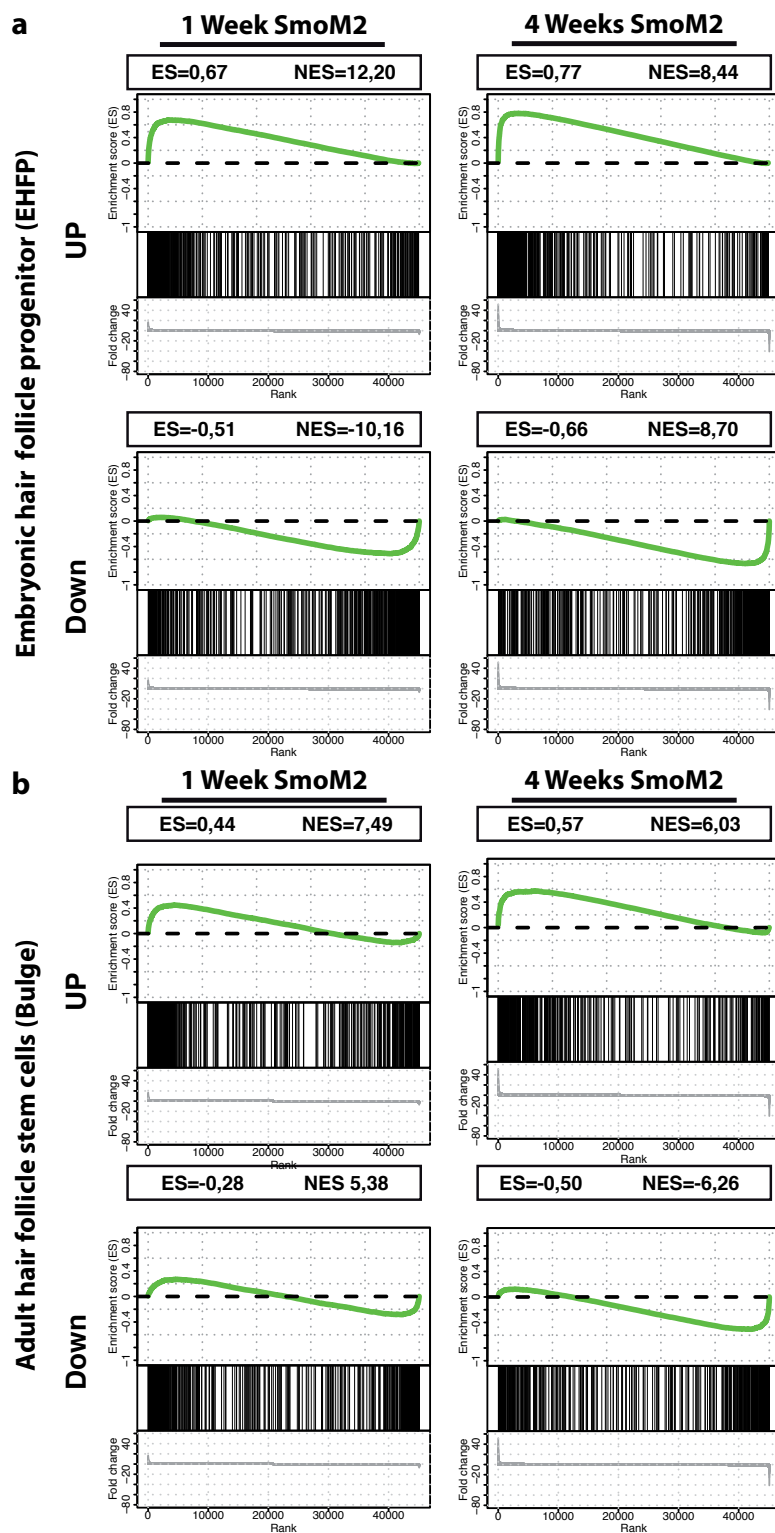


**Figure S2** GSEA analysis of the adult hair follicle bulge SC and EHFP gene signatures with the genes regulated by SmoM2. (a) Gene Set enrichment analysis (GSEA) showing the distribution of the EHFP upregulated (upper panel) or downregulated (bottom panel) genes sets within the rank order list of all the microarray gene set of the SmoM2-YFP+ FACS isolated tumor initiating cells ( $\alpha$ 6HCD34-) 1 week (left) and 4 weeks after SmoM2 expression (right).

(b) Gene Set enrichment analysis (GSEA) showing the distribution of the adult  $\alpha$ 6HCD34H bulge SC upregulated (upper panel) or downregulated (bottom panel) gene sets within the rank order list of all the microarray gene set of the SmoM2-YFP+ FACS isolated tumor initiating cells ( $\alpha$ 6HCD34-) one week (left) and four weeks after SmoM2 expression (right). Enrichment score (ES) and normalized enrichment Score (NES) are shown for each analysis.

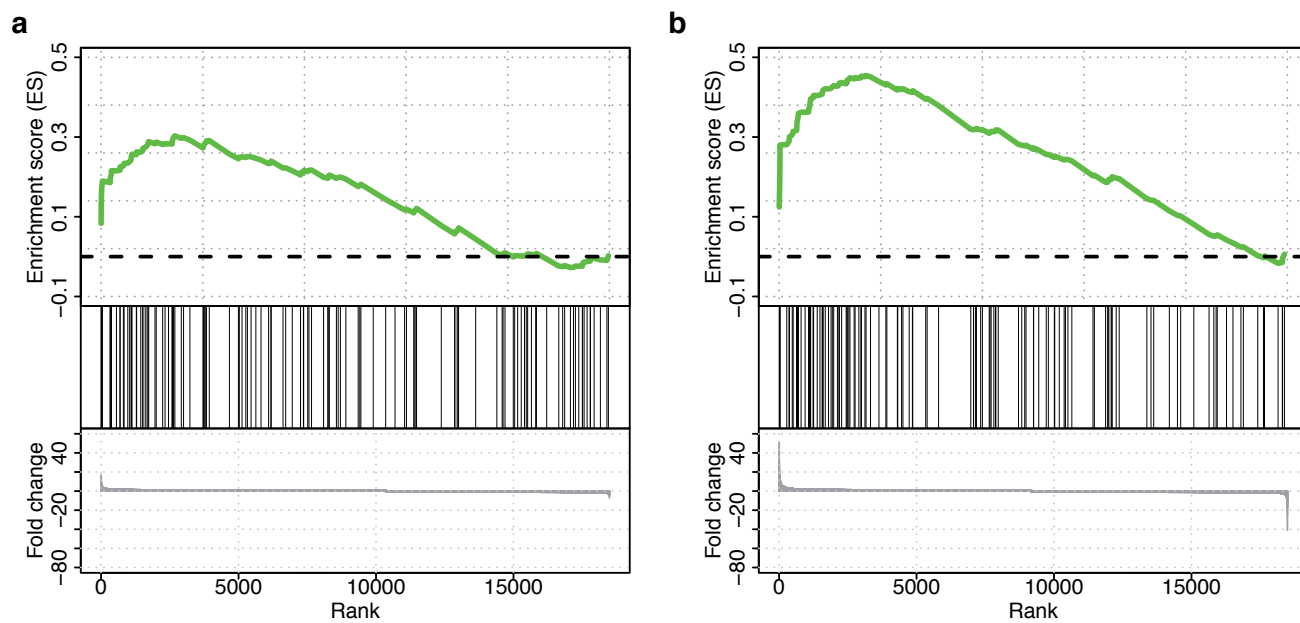


**Figure S3** Gene Ontology Enrichment (GO) analysis of SmoM2 signature gene. (a,b) GSEA showing the distribution of HH and canonical-Wnt GO enriched genes 1 week (c) and 4 weeks (d) after SmoM2 expression within the rank order list of microarray gene set.

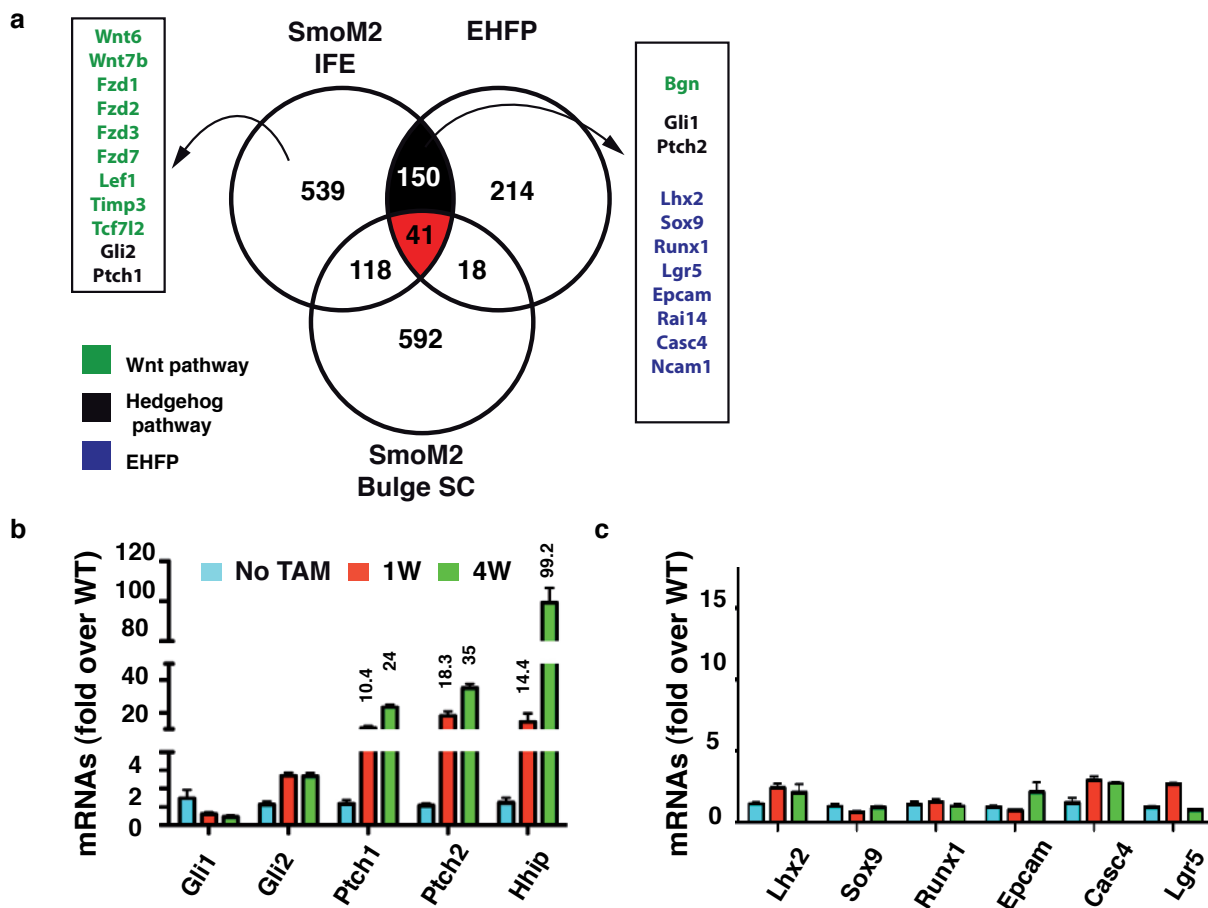


**Figure S4** Transcriptional profiling of FACS isolated bulge SC expressing SmoM2. (a) Venn diagram showing the similarities and the differences between the genes upregulated in the EHFP signature<sup>16</sup> and the genes upregulated by SmoM2 in adult IFE cells (a6HCD34-) and bulge SC (a6HCD34+) 4 weeks after SmoM2. The number of common genes between SmoM2 signature in bulge SC and EHFP signature decreases from 192 to 59 genes. The 150 genes highlighted in black represent the genes lost from the

common signature in the bulge SC. The 41 genes highlighted in red represent the genes upregulated by SmoM2 by more than 2 fold in both bulge SC and IFE cells. (b,c) Transcriptional analysis of HH target genes (b) and EHFP markers (c) in FACS isolated bulge SC (a6HCD34+) expressing SmoM2 cells one week and 4 weeks after 10 mg TAM administration to K19CREER/Rosa-SmoM2-YFP mice. The errors bars represent s.e.m. of the different replicates (control (No TAM, n=9), 1 week (n=6) and 4weeks (n=4)).

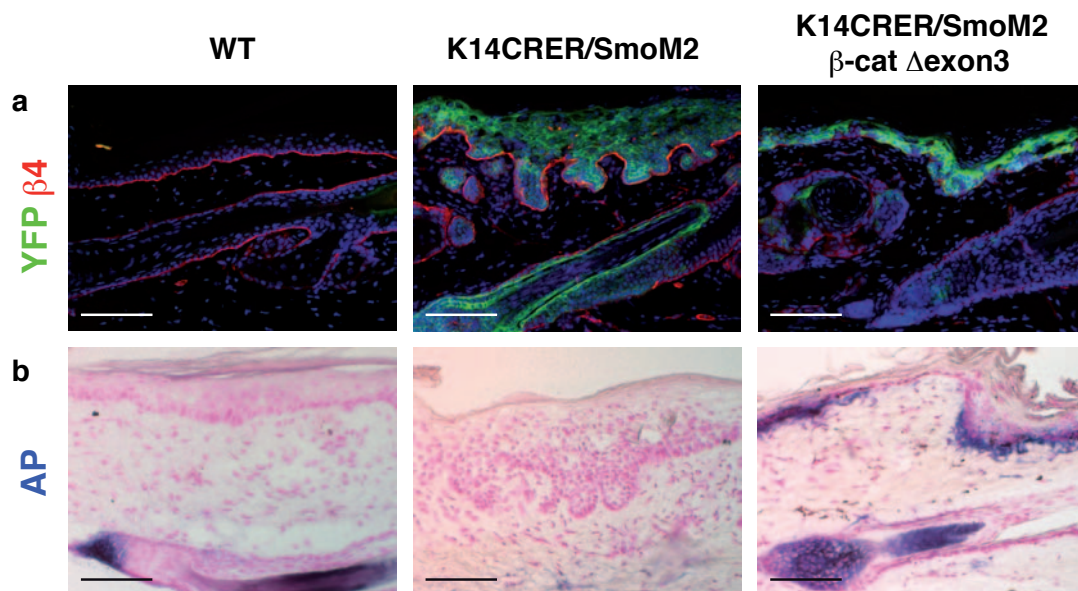


**Figure S5** Stabilized  $\beta$ -catenin expression inhibits the progression of SmoM2 induced tumors in the tail epidermis. (a-b) Immunostaining for  $\beta$ 4-integrin and SmoM2 (a) and alkaline phosphatase (AP) reaction (b) in wt, K14CREER/SmoM2-YFP and K14CREER/SmoM2-YFP/ $\beta$ catenin-

$\Delta$ exon3 tail epidermis 4 weeks after 15mg TAM administration showing a delay in tumor progression and the appearance of AP positive cells in the dermis of cells co-expressing SmoM2 and  $\beta$ catenin- $\Delta$ exon3. Scale bars, 50 $\mu$ m.

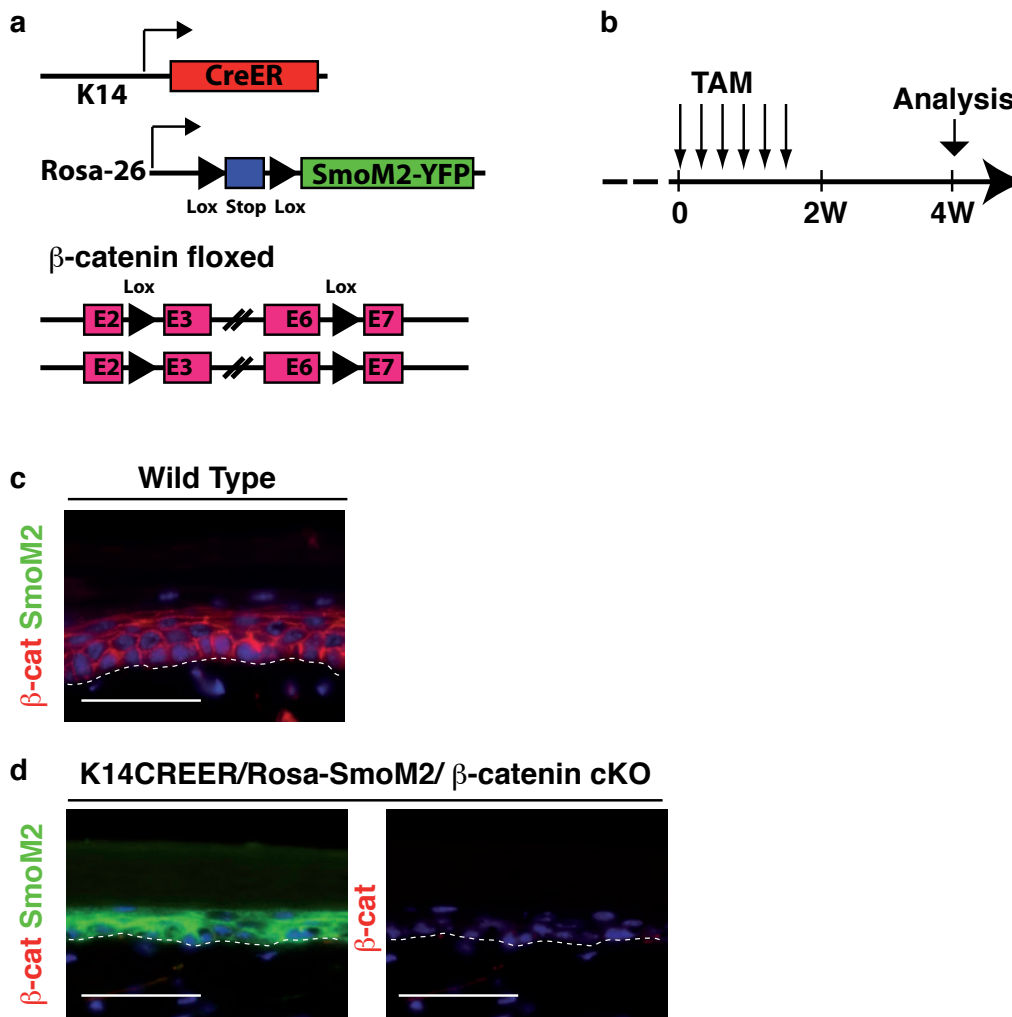


**Figure S6** Combined SmoM2 expression and  $\beta$ -catenin deletion in the adult skin epidermis. (a) Scheme representing the genetic strategy used to express SmoM2 in  $\beta$ -catenin deficient epidermal cells. (b) Scheme summarizing the protocol used to induce the SmoM2 expression and the deletion of

$\beta$ -catenin in adult interfollicular tail epidermis. (c, d) immunostaining of  $\beta$ -catenin (red) and SmoM2 (green) in the untreated tail epidermis (c) and 4 weeks after 15mg of TAM administration (d) in K14CREER /Rosa-SmoM2/  $\beta$ -catenin floxed/floxed mice. Scale bars, 50  $\mu$ m.

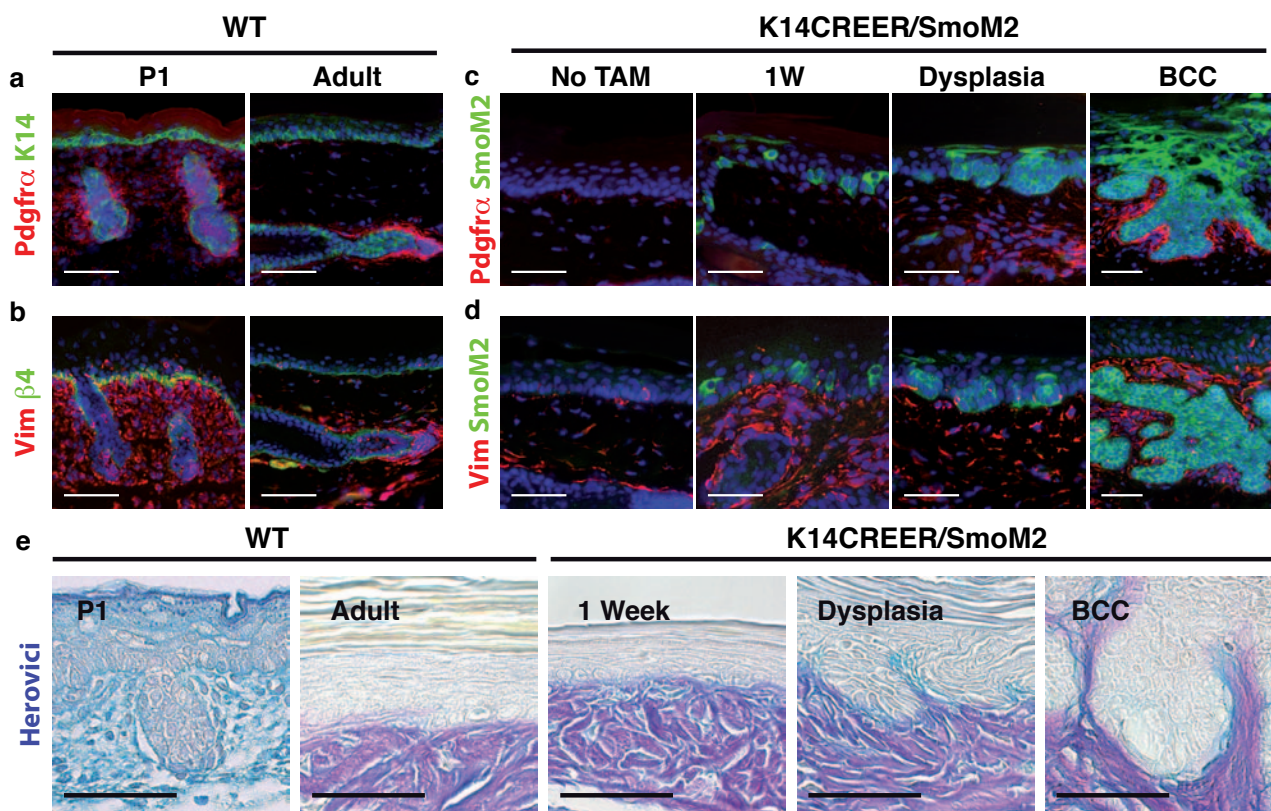


**Figure S7** Reprogramming of the dermis into an embryonic/neonatal stage following SmoM2 expression in the epidermis. (a-c) Immunostaining for Pdgfr $\alpha$  and K14 (a) and Vimentin and  $\beta$ 4-integrin (b) in neonatal and adult epidermis showing the enrichment of Pdgfr $\alpha$  and Vimentin in the neonatal dermis and their more restricted expression to the dermal papilla and mesenchymal cells surrounding the lower part of the hair follicle in the adult tail skin. (c, d) Immunostaining of Pdgfr $\alpha$  and

K14 (c) and Vimentin and  $\beta$ 4 (d) before, 1w, 4 weeks and 10 Weeks after TAM administration to K14CREER/SmoM2 mice. Note the strong increase of both Pdgfr $\alpha$  and Vimentin in the dermis cells following SmoM2 expression. (e) Herovici staining in neonatal and adult skin following SmoM2 expression. Note the appearance of light blue staining representing immature collagen fibers in the dermis underneath SmoM2 expressing epidermis. Scale bars, 50  $\mu$ m.

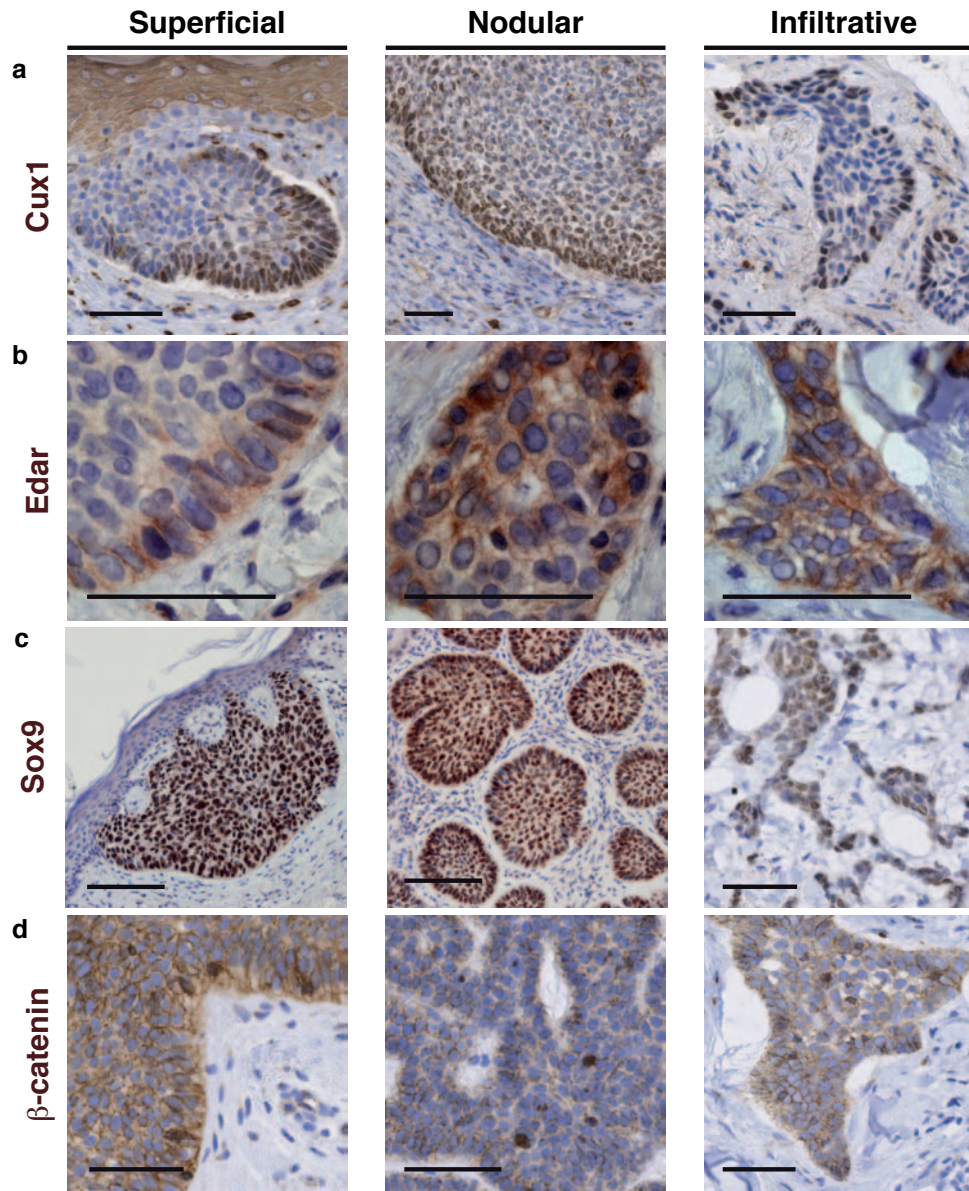


**Figure S8** Immunostaining of embryonic hair follicle progenitors and Wnt/ $\beta$ -catenin signaling markers in human basal cell carcinoma. (a-e) Immunostaining of embryonic hair follicle markers Cux1 (a), Edar (b), Sox9 (c) and  $\beta$ -catenin (d). Note the nuclear accumulation of  $\beta$ -catenin in all three BCC subtypes. Scale bars, 50  $\mu$ m